Chapter 2 in the book:
P.A. Kralchevsky and K. Nagayama, "Particles at Fluid Interfaces and Membranes"
(Attachment of Colloid Particles and Proteins to Interfaces and Formation of Two-Dimensional Arrays)
Elsevier, Amsterdam, 2001; pp. 64-104.

CHAPTER 2

INTERFACES OF MODERATE CURVATURE: THEORY OF CAPILLARITY

This chapter gives a brief presentation of the conventional theory of capillarity, which is based on the Laplace and Young equations, and neglects such effects as interfacial bending moment and curvature elastic moduli (the latter effects are subject of the next Chapter 3). The Laplace equation is derived by a force balance per unit area of a curved interface, as well as by means of a variational method. Various forms of Laplace equation are presented depending on the symmetry of the phase boundaries. Special attention is paid to the physically and practically important case of axisymmetric interfaces. Equations are given, which describe the shape of sessile and pendant drops, of the fluid interface around a vertical cylinder, floating solid or fluid particle, hole in a wetting film, capillary "bridges", Plateau borders in foams, the profile of the free surface of a fluid particle or biological cell pressed between two plates, etc.

The values of the contact angles subtended between three intersecting surfaces are determined by the force balance at the contact line, which is given by the Young and Neumann equations. It is demonstrated that these equations (likewise the Laplace equation) can be derived by variation of the thermodynamic potential. The rule how to calculate the net force exerted on a particle at an interface is discussed. Linear excess energy (line tension) can be ascribed to a contact line. When the contact line is curved, the line tension gives a contribution to the Young and Neumann equations. The presence of line tension effect is indicated by dependence of the contact angle on the curvature of the contact line. The contact angles can vary also due to the phenomenon hysteresis, which is considered in relation to the line tension effect.

The chapter represents a basis for most of the subsequent chapters since the subjects of first importance in this book are the shapes of the menisci around attached particles, the shapes of fluid particles approaching an interface, the balances of forces exerted on particles at interfaces, and various kinds of capillary forces.

2.1. THE LAPLACE EQUATION OF CAPILLARITY

2.1.1. LAPLACE EQUATION FOR SPHERICAL INTERFACE

Let us consider a spherical interface between two fluid phases (spherical liquid drop or gas bubble). In Fig. 2.1 P_1 and P_2 denote the inner and outer pressure, respectively; R is the radius of the spherical dividing surface (defined as the surface of tension) and σ is the interfacial tension. Let us make the balance of all forces exerted on a small segment of the dividing surface situated around its intersection point with the z-axis (Fig. 2.1) and corresponding to a central angle θ. The area of this segment is

$$A(\theta) = 2\pi R^2(1 - \cos\theta) \approx \pi R^2\theta^2 \qquad (\theta << 1) \tag{2.1}$$

The length of the circumference encircling this segment is

$$L(\theta) = 2\pi R\sin\theta \approx 2\pi R\theta \qquad (\theta << 1) \tag{2.2}$$

Then the balance of the forces acting on the segment, resolved along the z-axis, reads:

$$P_1 A(\theta) = P_2 A(\theta) + (\sigma\sin\theta) L(\theta) \tag{2.3}$$

The left-hand side of Eq. (2.3) represents the force directed upwards, whereas the right-hand side expresses the forces acting downwards (Fig. 2.1); these forces should counterbalance each other for an equilibrium interface. Substituting Eqs. (2.1) and (2.2) into Eq. (2.3), and carrying out the transition $\theta \to 0$, one obtains the *Laplace equation* of capillarity for a spherical interface [1]:

$$\frac{2\sigma}{R} = P_1 - P_2 \tag{2.4}$$

Equation (2.4) shows that the pressure exhibits a jump,

$$P_c = P_1 - P_2 \tag{2.5}$$

across a spherical interface; P_c is called *capillary* pressure, or Laplace pressure. In the limit $R \to 0$ (planar interface) Eq. (2.4) yields $P_1 = P_2$, as this must be for a flat dividing surface, see

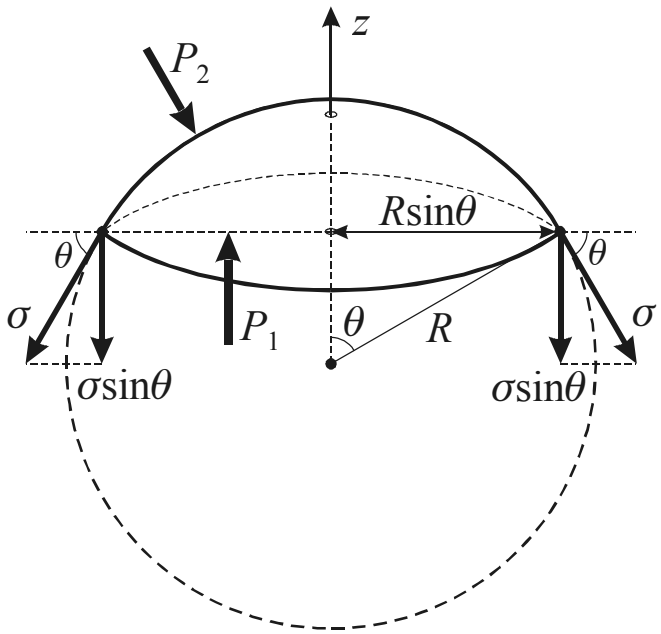

Fig. 2.1. Balance of forces exerted on a segment of spherical interface or membrane of tension σ and radius R; the segment is encompassed by the circumference of radius $R\sin\theta$, where θ is a central angle; P_1 and P_2 denote the inner and outer pressure, respectively.

Section 1.1. The above purely hydrostatic derivation of the Laplace equation reveals its physical meaning: it expresses the normal force balance per unit area of the interface. Below we proceed with the derivation of the form of Laplace equation for an arbitrarily curved interface.

2.1.2. General form of Laplace equation

Derivation by minimization of the grand potential. Let us consider a two-phase fluid system confined in a box of volume V, see Fig. 2.2. The volumes of the two phases are V_1 and V_2 ; we have $V_1 + V_2 = V$. We assume also that the chemical potentials of all components in the system are kept constant. Then the equilibrium state of the system corresponds to a minimum of the grand thermodynamic potential, Ω [2-4]:

$$\Omega = -\int_{V_1} P_1 dV - \int_{V_2} P_2 dV + \sigma A \tag{2.6}$$

where A is the area of the interface; the pressures P_1 and P_2 depend on the vertical coordinate z due to the effect of gravity:

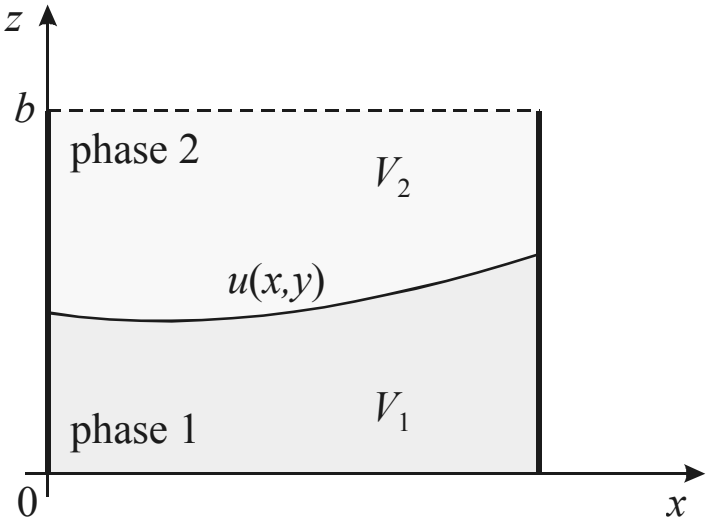

Fig. 2.2. Sketch of a two-phase system composed of phases 1 and 2, which occupy volumes V_1 and V_2, respectively; $z = u(x,y)$ is the equation of the phase boundary.

$$P_1(z) = P_{10} - \rho_1 g z, \qquad P_2(z) = P_{20} - \rho_2 g z, \tag{2.7}$$

P_{10} and P_{20} are constants, ρ_1 and ρ_2 are the mass densities of the two neighboring fluids, and g is the acceleration due to gravity. Let $z = u(x,y)$ to be the equation describing the shape of the interface. Then the area of the interface is

$$A = \int_{A_0} dxdy\sqrt{1+u_x^2+u_y^2}, \qquad u_x \equiv \frac{\partial u}{\partial x}, \qquad u_y \equiv \frac{\partial u}{\partial y} \tag{2.8}$$

A_0 is the projection of the interface on the coordinate plane xy. In addition, one derives

$$\int_{V_1} P_1(z)dV = \int_{A_0} dxdy \int_0^{u(x,y)} dz\, P_1(z), \qquad \int_{V_1} P_2(z)dV = \int_{A_0} dxdy \int_{u(x,y)}^{b} dz\, P_2(z), \tag{2.9}$$

where $z = 0$ and $z = b$ are the lower and the upper side of the box (Fig. 2.2). The substitution of Eqs. (2.8) and (2.9) into Eq. (2.6) yields

$$\Omega = \int_{A_0} dxdy L\big(u(x,y), u_x(x,y), u_y(x,y)\big) \tag{2.10}$$

where

$$L(u,u_x,u_y) \equiv -\int_0^u P_1(z)dz - \int_u^b P_2(z)dz + \sigma\sqrt{1+u_x^2+u_y^2} \tag{2.11}$$

Equations (2.10) and (2.11) show that the grand potential Ω depends as a functional on the interfacial shape $u(x,y)$. Then the necessary condition for minimum of Ω is given by the known Euler equation [5,6]:

$$\frac{\partial L}{\partial u} - \frac{\partial}{\partial x}\frac{\partial L}{\partial u_x} - \frac{\partial}{\partial y}\frac{\partial L}{\partial u_y} = 0 \tag{2.12}$$

Differentiating Eq. (2.11) one obtains

$$\frac{\partial L}{\partial u} = -P_1(u) + P_2(u) \tag{2.13}$$

Next, differentiating Eq. (2.11) one can derive

$$\frac{\partial}{\partial x}\frac{\partial L}{\partial u_x} + \frac{\partial}{\partial y}\frac{\partial L}{\partial u_y} = 2H\sigma \tag{2.14}$$

where we have used the notation

$$2H \equiv \nabla_{\mathrm{II}} \cdot \left(\frac{\nabla_{\mathrm{II}} u}{\sqrt{1 + \left|\nabla_{\mathrm{II}} u\right|^2}} \right) \tag{2.15}$$

$$\nabla_{\mathrm{II}} \equiv \mathbf{e}_x \frac{\partial}{\partial x} + \mathbf{e}_y \frac{\partial}{\partial y} \tag{2.16}$$

Here ∇_{II} is the two-dimensional gradient operator in the plane xy; H defined by Eq. (2.15) is a basic quantity in differential geometry, which is termed *mean curvature* of the surface [5,7,8]. Note that Eq. (2.15) is expressed in a covariant form and can be specified for any type of curvilinear coordinates in the plane xy (not only Cartesian ones). Substituting Eqs. (2.13) and (2.14) into Eq. (2.12) we obtain a general form of Laplace equation of capillarity [1]:

$$2H\sigma = P_2(u) - P_1(u) \qquad \text{(Laplace equation)} \tag{2.17}$$

When the pressures P_1 and P_2 are dependent on the position in space, as it is in Eq. (2.7), their values *at the interface* enter the Laplace equation; in such a case the capillary pressure, $P_c \equiv P_1(u) - P_2(u)$, varies throughout the interface.

Various forms of Laplace equation. The mean curvature can be expressed through the two principle radii of curvature of the surface, R_1 and R_2 [5,7]:

$$H = -\frac{1}{2}\left(\frac{1}{R_1} + \frac{1}{R_2}\right) \tag{2.18}$$

Combining Eqs. (2.17) and (2.18) one obtains another popular form of Laplace equation [9]:

$$\sigma\left(\frac{1}{R_1} + \frac{1}{R_2}\right) = P_1(u) - P_2(u) \qquad \text{(Laplace equation)} \tag{2.19}$$

For a spherical interface the two principal radii of curvature are equal, $R_1 = R_2 = R$, and then Eq. (2.19) reduces to Eq. (2.4). The original form of Eq. (2.17), published by Laplace in 1805, can be obtained if the right-hand side of Eq. (2.15) is expressed in Cartesian coordinates and the differentiation is carried out [1]:

$$\frac{\left(1+u_y^2\right)u_{xx} - 2u_{xy}u_x u_y + \left(1+u_x^2\right)u_{yy}}{\left(1+u_x^2+u_y^2\right)^{3/2}} = [P_2(u) - P_1(u)]/\sigma \tag{2.20}$$

Here u_{xx}, u_{xy} and u_{yy} denote the respective second derivatives of $u(x,y)$. One sees that in general the Laplace equation, Eq. (2.20), is a second order non-linear partial differential equation for determining the shape of the fluid phase boundary, $u(x,y)$. The way we derived Eq. (2.20) shows that its solution, $u(x,y)$, minimizes the grand thermodynamic potential, Ω, and consequently, corresponds to the state of mechanical equilibrium of the system. For interfaces of rotational or translational symmetry Eq. (2.20) reduces to an ordinary differential equation (see below), which is much easier to solve.

If the curved interface in Fig. 2.2 has *translational* symmetry along the y-axis, i.e. $z = u(x)$, then $u_y = 0$, $u_{xy} = u_{yy} = 0$, and Eq. (2.20) reduces to:

$$\frac{u_{xx}}{\left(1+u_x^2\right)^{3/2}} = (P_2 - P_1)/\sigma \qquad \text{(translational symmetry)} \tag{2.21}$$

If the curved interface has *rotational* symmetry around the z-axis (axial symmetry), then it is convenient to introduce polar coordinates (r,φ) in the plane xy. Due to the axial symmetry the

equation of the interface has the form $z = u(r)$. Then introducing polar coordinates in Eq. (2.15) one can bring Eq. (2.17) into the form [10]:

$$\frac{1}{r}\frac{d}{dr}\left[\frac{r u_r}{\left(1+u_r^2\right)^{1/2}}\right] = (P_2 - P_1)/\sigma \qquad \text{(rotational symmetry)} \qquad (2.22)$$

where $u_r \equiv du/dr$. Sometimes it is more convenient to work in terms of the inverse function of $z = u(r)$, that is $r = r(z)$. In such a case Eq. (2.22) can be transformed in an equivalent form [10,11]:

$$-\frac{r_{zz}}{(1+r_z^2)^{3/2}} + \frac{1}{r(1+r_z^2)^{1/2}} = \frac{P_2 - P_1}{\sigma}, \qquad r_z \equiv \frac{dr}{dz}, \qquad r_{zz} \equiv \frac{d^2 r}{dz^2} \qquad (2.23)$$

Two equivalent parametric forms of Laplace equation are often used for analytical and numerical calculations [10,11]:

$$\frac{d\sin\varphi}{dr} + \frac{\sin\varphi}{r} = \frac{P_c}{\sigma}, \qquad \tan\varphi = \pm\frac{dz}{dr} \qquad (2.24)$$

(the angle φ can be defined with both positive or negative sign) and

$$\frac{d\varphi}{ds} = \frac{P_c}{\sigma} - \frac{\sin\varphi}{r}, \qquad \frac{dr}{ds} = \cos\varphi, \qquad \frac{dz}{ds} = \sin\varphi \qquad (2.25)$$

Here φ is the meniscus running slope angle and s is the arc length along the generatrix of the meniscus $z = z(r)$; P_c is the capillary pressure defined by Eq. (2.7); the sign of P_c is to be specified for every given interface. Equations (2.25) represent a set of three equations for determining the functions $\varphi(s)$, $r(s)$ and $z(s)$, which is especially convenient for numerical integration [11]; note that Eq. (2.24) may create numerical problems at the points with $\tan\varphi = \pm\infty$, like the points on the "equator" of the fluid particle in Fig. 2.3.

The Laplace equation can be generalized to account for such effects as the interfacial bending elasticity and shearing tension; such a generalization is important for interfaces and membranes of low tension and high curvature and can be used to describe the configurations of red blood cells, see Chapters 3 and 4.

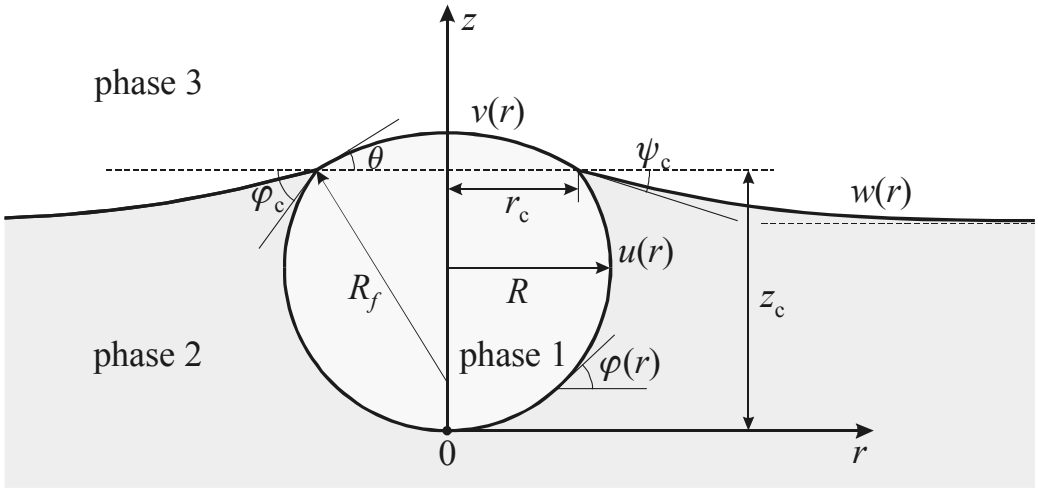

Fig. 2.3. Cross-section of a light fluid particle (bubble or droplet) from Phase 1, which is attached to the boundary between Phases 2 and 3. The equations of the boundaries between phases 1-2, 1-3 and 2-3 are denoted by $u(r)$, $v(r)$ and $w(r)$, respectively; φ_c, θ and ψ_c are slope angles of the respective phase boundaries at the contact line, which intersects the plane of the drawing in the point (r_c,z_c); $\varphi(r)$ is a running slope angle; R is "equatorial" radius and R_f is the curvature radius of the surface $v(r)$, which can be a thin film of Phase 2, intervening between Phases 1 and 3.

2.2. AXISYMMETRIC FLUID INTERFACES

Very often the boundaries between two fluid phases (the capillary menisci) have rotational (axial) symmetry. An example is the fluid particle (drop or bubble) attached below an interface,

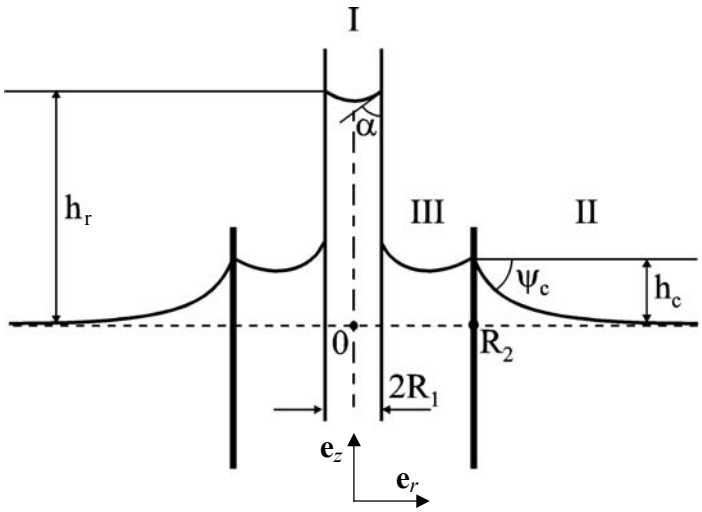

Fig. 2.4. Menisci formed by the liquid around two vertical coaxial cylinders of radii R_1 and R_2: (I) Meniscus meeting the axis of revolution; (II) Meniscus decaying at infinity; (III) Meniscus confined between the two cylinders; h_r is the capillary rise in the inner cylinder; h_c and ψ_c are the elevation and the slope angle of Meniscus II at the contact line $r = R_2$.

which is depicted in Fig. 2.3: all interfaces, $u(r)$, $v(r)$ and $w(r)$, have axial symmetry. In general, there are three types of axially symmetric menisci corresponding to the three regions denoted in Fig. 2.4: (I) Meniscus meeting the axis of revolution, (II) Meniscus decaying at infinity, and (III) Meniscus confined between two cylinders, $0 < R_1 < r < R_2 < \infty$; see e.g. Ref. [10,12]. These three cases are separately considered below.

2.2.1. MENISCUS MEETING THE AXIS OF REVOLUTION

The interfaces $u(r)$ and $v(r)$ in Fig. 2.3 belong to this type of menisci, as well as the interfaces of floating lenses and any kind of sessile or pendant drops/bubbles. Such a meniscus is a part of a sphere when the effect of gravity is negligible, that is when the capillary (or Bond) number is small:

$$\beta_c \equiv g b^2 \Delta\rho / \sigma << 1 \tag{2.26}$$

Here, as usual, g is the acceleration due to gravity, $\Delta\rho$ is the magnitude of the difference in the mass densities of the two fluids and b is a characteristic radius of the meniscus curvature. For example, if Eq. (2.26) is satisfied with $b = R_1$, see Region I in Fig. 2.4, the *capillary rise*, h_r, of the liquid in the inner cylinder is determined by means of the equation [13]

$$h_r = (2\sigma\cos\alpha)/(\Delta\rho\, g\, R_1) \tag{2.27}$$

α is a contact angle which can be both acute and obtuse, depending on whether the inner surface of the cylinder is hydrophilic or hydrophobic; in the case $\alpha > 90°$ h_r becomes negative and the inner meniscus is situated below the level of the outer liquid far from the cylinders in Fig. 2.4.

To obtain the equations for the shape of the lower interface, $u(r)$, of the fluid particle in Fig. 2.3 let us fix the coordinate origin at the bottom of the particle. Combining Eqs. (2.5), (2.7), (2.24) and (2.26) one can obtain the Laplace equation in the form:

$$\frac{d\sin\varphi}{dr} + \frac{\sin\varphi}{r} = \frac{2}{b} + \varepsilon\frac{\beta_c}{b^2} z, \qquad \tan\varphi = -\frac{dz}{dr}; \qquad b \equiv \frac{2\sigma}{P_{10} - P_{20}} \tag{2.28}$$

Here b is the radius of curvature at the bottom of the bubble (drop) surface, where $z = 0$, see Fig 2.3; the parameter ε takes values ±1. For *sessile* type drops or bubbles the mass density of the

fluid particle (Phase 1) is smaller than that of Phase 2, $\rho_1 < \rho_2$, and $\varepsilon = +1$; for *pendant* type drops/bubbles $\rho_1 > \rho_2$ and $\varepsilon = -1$. The definition of the sign of $\tan\varphi$ in Eq. (2.28) leads to

$$\varphi = \pi \quad \text{at} \quad z = 0. \tag{2.29}$$

Equations (2.28) allow one to determine the meniscus profile in a parametric form, that is $r = r(\varphi)$ and $z = z(\varphi)$. Let us consider three cases corresponding to different values of the capillary number β_c.

(i) No gravity deformation: $\beta_c = 0$. Such is the case of small fluid particles (drops, bubbles) for which the gravitational deformation can be neglected. In this case the only solution of the Laplace equation, Eq. (2.28), is a *spherical* meniscus:

$$\frac{r(\varphi)}{b} = \sin\varphi; \qquad \frac{z(\varphi)}{b} = 1 + \cos\varphi. \tag{2.30}$$

If the boundaries of small fluid particles or biological cells have a shape, which is different from spherical, this is an indication about the presence of an effect of the interfacial (membrane) bending elasticity, see Chapter 3.

(ii) Small gravity deformation: $\beta_c << 1$. In this case the solution of Eq. (2.28) can be obtained as truncated asymptotic expansions with respect to the powers of β_c, see Ref. [14]:

$$\begin{aligned}\frac{r(\varphi)}{b} &= \sin\varphi + \varepsilon\beta_c\left(\tfrac{1}{3}\cot\frac{\varphi}{2} - \tfrac{1}{6}\sin 2\varphi - \tfrac{1}{2}\sin\varphi\right) \\ &+ \beta_c^2\left[\left(\tfrac{3}{4} + \tfrac{1}{2}\cos\varphi - \tfrac{2}{9}\sin^2\varphi - \tfrac{1}{3}\ln\sin\frac{\varphi}{2}\right)\sin\varphi - \tfrac{1}{2}\left(1 + \tfrac{1}{9}\cot^2\frac{\varphi}{2}\right)\cot\frac{\varphi}{2}\right]\end{aligned} \tag{2.31}$$

$$\frac{z(\varphi)}{b} = 1 + \cos\varphi + \varepsilon\beta_c\left[\tfrac{1}{3}\sin^2\varphi + \tfrac{2}{3}\ln\sin\frac{\varphi}{2} - \tfrac{1}{2}(1 + \cos\varphi)\right] \qquad (15° \le \varphi \le 180°) \tag{2.32}$$

For $\beta_c \to 0$ Eqs. (2.31) and (2.32) reduce to Eq. (2.30). Equations (2.31) and (2.32) are applicable with a good accuracy for $15° < \varphi \le 180°$, see Refs. [14,15] for details. In the case when $0° \le \varphi \le 15°$ instead of Eqs. (2.31) and (2.32) one can use the following asymptotic expansions [14,15]:

$$\frac{r}{b} = p - \frac{27p^7 + 108\varepsilon\beta_c p^5 + 144\beta_c^2 p^3 - 8\varepsilon\beta_c^3 p}{54\left(3p^4 + 2\varepsilon\beta p^2\right)} + O(\beta_c^2) \tag{2.33}$$

$$\frac{z}{b} = 2 - \tfrac{1}{2}\varphi\, p + \tfrac{2}{3}\varepsilon\,\beta_c \ln\frac{p}{2\mathrm{e}} + O(\beta_c^2) \qquad (0° \le \varphi \le 15°) \tag{2.34}$$

where e is the Napier number, ln(e) = 1, and $p \equiv \tfrac{1}{2}\left(\varphi + \sqrt{\varphi^2 + \tfrac{8}{3}\varepsilon\beta_c}\right)$, see Ref. [15] for more details.

Other approximate solutions of Laplace equation can be found in Refs. [11,16]. For example, if the meniscus slope is small, $u_r^2 << 1$, Eq. (2.22) reduces to a linear differential equation of Bessel type, whose solution reads

$$z(r) = u(r) = 2[\mathrm{I}_0(qr) - 1]/(bq^2), \qquad q \equiv (\Delta\rho g/\sigma)^{1/2}, \qquad u_r^2 << 1 \tag{2.35}$$

where $\mathrm{I}_0(x)$ is the modified Bessel function of the first kind and zeroth order [5,17,18].

(iii) The gravity deformation is considerable and β_c is not a small parameter. In this case one can integrate numerically the Laplace equation in its parametric presentation, Eq. (2.25).

Despite the fact that in the presence of gravitational deformation the Laplace equation has no exact analytical solution, it is curious to note that there is an exact formula for the *volume* of a sessile or pendant drop (bubble), irrespective of the magnitude of the gravitational deformation. For example, the volume V_1 of the lower part of the drop (bubble) in Fig. 2.3, that is comprised between the planes $z = 0$ and $z = z_c$, is

$$V_1 = \int_0^{2\pi} d\omega \int_0^{z_c} dz \int_0^{r(z)} r dr = \pi \int_0^{z_c} dz r^2(z) = \pi z_c r_c^2 - 2\pi \int_0^{z_c} dz\, z r(z) \frac{dr}{dz} \tag{2.36}$$

Here ω denotes the azimuthal angle in the plane xy, $r = r(z)$ is the generatrix of the interfacial profile, r_c is the radius of the contact line (Fig. 2.3); at the last step in Eq. (2.36) we have integrated by parts. On the other hand, Eq. (2.28) can be expressed in the form

$$\frac{d}{dr}(r\sin\varphi) = \frac{2}{b} r + \varepsilon\, q^2 z\, r \tag{2.37}$$

where q is defined by Eq. (2.35). Next, one multiplies Eq. (2.37) by dr/dz and integrates for $0 \le z \le z_c$; in view of Eq. (2.29) the result reads:

$$r_c \sin\varphi_c = \frac{r_c^2}{b} + \varepsilon q^2 \int_0^{z_c} dz\, z\, r(z) \frac{dr}{dz} \tag{2.38}$$

The integral in Eqs. (2.36) and (2.38) cannot be solved analytically; however, this integral can be eliminated between these two equations to obtain

$$V_1 = \pi z_c r_c^2 + \frac{2\pi}{\varepsilon q^2}\left(\frac{r_c^2}{b} - r_c \sin\varphi_c\right) \tag{2.39}$$

where φ_c is the value of the slope angle φ at $z = z_c$, see Fig. 2.3. Similar expression can be obtained also for the volume V_2 of the upper part of the fluid particle in Fig. 2.3, that part situated above the plane $z = z_c$.

2.2.2. MENISCUS DECAYING AT INFINITY

Examples are the outer meniscus, $z = w(r)$ in Fig. 2.3 and the meniscus in the outer Region II in Fig. 2.4. In this case the action of gravity cannot be neglected insofar as the gravity keeps the interface flat far from the contact line. Let $z = 0$ be the equation of the aforementioned flat interface. Then $P_{10} = P_{20}$ in Eq. (2.7) and the capillary pressure is $P_c = \Delta\rho g z$; the Laplace equation (2.22) for the function $z(r)$ takes the form:

$$\frac{z_{rr}}{\left(1+z_r^2\right)^{3/2}} + \frac{z_r}{r\left(1+z_r^2\right)^{1/2}} = q^2 z\,, \qquad z_r \equiv \frac{dz}{dr}, \qquad z_{rr} \equiv \frac{d^2 z}{dr^2} \tag{2.40}$$

Equation (2.40) has no closed analytical solution. The region far from the contact line has always small slope, $z_r^2 << 1$. In this region Eq. (2.40) can be linearized and reduces to a modified Bessel equation; in analogy with Eq. (2.35) one derives

$$z(r) = A\, \mathrm{K}_0(qr) \qquad (z_r^2 << 1) \tag{2.41}$$

where A is a constant of integration and $\mathrm{K}_0(x)$ is the modified Bessel function of the second kind and zeroth order [5,17,18]. The numerical integration of Eq. (2.40) can be carried out by

using Eq. (2.41) as a boundary condition, together with $z_r = -qA\mathrm{K}_1(qr)$ for some appropriately fixed $r >> q^{-1}$ [11]; the constant A is to be determined from the boundary condition at $r = \mathrm{R}_2$.

Approximate analytical solutions of the problem are available [14,19–21]. For the case, when the radius of the contact line R_2 (Fig. 2.4) is much smaller than the characteristic capillary length, q^{-1}, Derjaguin [19] has derived an asymptotic formula for the elevation of the contact line at the outer surface of the cylinder $r = R_2$:

$$h_c = -R_2 \sin\psi_c \ln[qR_2\gamma_e(1+\cos\psi_c)/4], \qquad (qR_2)^2 << 1 \qquad (2.42)$$

Here ψ_c is the meniscus slope angle at the contact line (Fig. 2.4), q is defined by Eq. (2.35) and $\gamma_e = 1.781\ 072\ 418...$ is the Euler constant [17]. Note that Derjaguin's formula (2.42) is valid not only in the case $0 \le \psi_c \le 90°$, but also in the case $90° \le \psi_c \le 180°$, in which the meniscus has

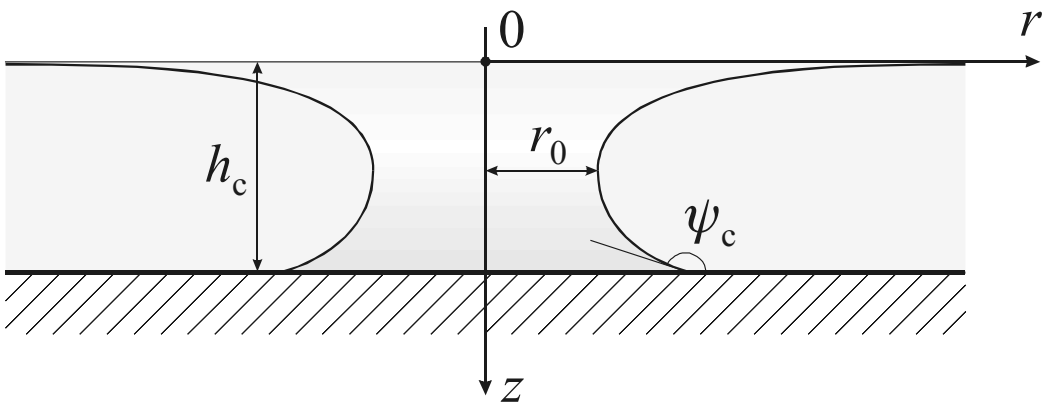

Fig. 2.5. Sketch of a circular hole in a liquid wetting film of thickness h_c on a solid substrate; ψ_c is the contact angle and r_0 is the radius of the "neck" of the meniscus.

a neck, see e.g. Fig. 2.5. If the condition $(qR_2)^2 << 1$ is satisfied, the constant A in Eq. (2.41) can be determined [19,14]:

$$z(r) = R_2 \sin\psi_c \mathrm{K}_0(qr) \qquad z_r^2 << 1, \qquad (qR_2)^2 << 1 \qquad (2.43)$$

Particles floating on a fluid interface of entrapped in a liquid film usually create small interfacial deformations, for which Eqs. (2.42) and (2.43) are applicable. These equations will be used below in this book to describe quantitatively the lateral capillary forces due to the overlap of the interfacial deformations (menisci) formed around such particles.

If the condition $z_r^2 << 1$ is not fulfilled close to the cylinder $r = R_2$, in this region one can use an alternative "inner" asymptotic expression [14],

$$z(r) = h_c - \sin\psi_c \left[\operatorname{arccosh}\left(\frac{r}{R_2 \sin\psi_c} \right) - \operatorname{arccosh}\left(\frac{1}{\sin\psi_c} \right) \right] \qquad (qR_2)^2 << 1 \qquad (2.44)$$

In Eq. (2.44) $r \geq R_2$ and h_c is given by Eq. (2.42); $\operatorname{arccosh} x = \ln[x + (x^2 - 1)^{1/2}]$; Eq. (2.44) has meaning for $z > 0$. For large values of r Eq. (2.44) predicts negative values of $z(r)$, which indicates that this asymptotic formula is out of the region of its validity. Higher order correction terms in Eqs. (2.42)–(2.44) are derived in Refs. [14,20].

If the thickness h_c of the liquid film in Fig. 2.5 is small enough one can use $(qh_c)^2$ as a small parameter and to obtain asymptotic expansions for the meniscus profile. In this way O'Brien [21] has derived an expression for the radius of the "neck", r_0 (the meniscus has a vertical tangent at $r = r_0$):

$$r_0 = - h_c \{ \ln[\tfrac{1}{4} q\, r_0\, \gamma_e \cot(\psi_c/2)] \}^{-1} \qquad (qh_c)^2 << 1, \qquad 90° \leq \psi_c < 180°. \qquad (2.45)$$

For given h_c and ψ_c the radius of the "neck" (or "pinhole") r_0 can be calculated from Eq. (2.45) by iterations. For $\psi_c = 90°$ the radii of the neck and contact line coincide, $r_0 \equiv R_2$, and in this special case Eqs. (2.42) and (2.45) coincide. For $\psi_c \to 180°$ the asymptotic formula (2.45) is not valid and another procedure of calculations is suggested in Ref. [21]; alternatively, Eq. (2.25) with $P_c = \Delta\rho g z$ can be integrated numerically.

2.2.3. MENISCUS CONFINED BETWEEN TWO CYLINDERS, $0 < R_1 < r < R_2 < \infty$

This type of capillary menisci include the various capillary bridges (Fig. 2.6a), the channels (borders) in foams and some emulsions, as well as the borders around the model thin liquid films in the experimental cells of Scheludko [22-24] and Mysels [25]; such is the configuration of fluid particles or biological cells pressed between two surfaces, see Fig. 2.6b and Refs. [26,27]. The shape of these menisci have been first investigated by Plateau [28] and Gibbs [29] in connection to the borders in the foams

If the gravitational deformation of the meniscus cannot be neglected, the interfacial shape can be determined by numerical integration of Eq. (2.25), or by iterative procedure [30]. If the meniscus deformation caused by gravity is negligible, analytical solution can be found as described below. Equation (2.24) can be presented in the form

$$\frac{d}{dr}(r\sin\varphi) = 2k_1 r, \qquad k_1 \equiv \frac{P_1 - P_2}{2\sigma} \tag{2.46}$$

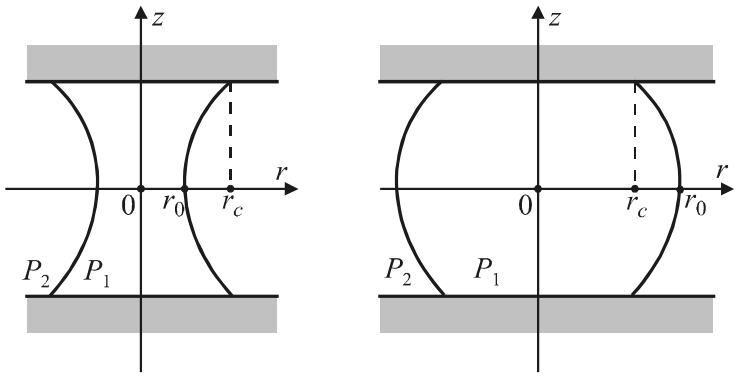

(a) (b)

Fig. 2.6. Capillary bridges between two parallel plates: (a) concave bridge, (b) convex bridge; r_c is the radius of the three-phase contact line; r_0 is the radius of the section with the plane of symmetry; P_1 and P_2 are the pressures inside and outside the bridge, respectively.

The pressures in phases 1 and 2, P_1 and P_2, and the coordinate of the point with vertical tangent, r_0, are shown in Fig. 2.6. To determine the shape of the menisci depicted in Figs. 2.6a and 2.6b we integrate Eq. (2.46) from r_0 to r to derive

$$\sin\varphi = k_1 r + \frac{r_0}{r}(1 - k_1 r_0) \tag{2.47}$$

Next, using Eq. (2.47) and the identity $\tan\varphi = \pm\sin\varphi/(1-\sin^2\varphi)^{1/2}$ one obtains

$$\frac{\mathrm{d}z}{\mathrm{d}r} = \frac{k_1\left(r^2 - r_0^2\right) + r_0}{\pm\left[\left(r^2 - r_0^2\right)\left(r_1^2 - r^2\right)\right]^{1/2}|k_1|}, \qquad r_1 \equiv \left|\frac{1 - k_1 r_0}{k_1}\right| \tag{2.48}$$

Equation (2.48) describes curves, which after Plateau [28,31,10] are called "nodoid" and "unduloid," see Fig. 2.7. One sees that the nodoid (unlike the unduloid) has points with horizontal tangent, where $\mathrm{d}z/\mathrm{d}r = 0$. With the help of Eq. (2.48) one can deduce that the

meniscus generatrix is a part of *nodoid* for $k_1 r_0 \in (-\infty, 0) \cup (1, +\infty)$, whereas the meniscus generatrix is a part of *unduloid* for $k_1 r_0 \in (0, 1)$.

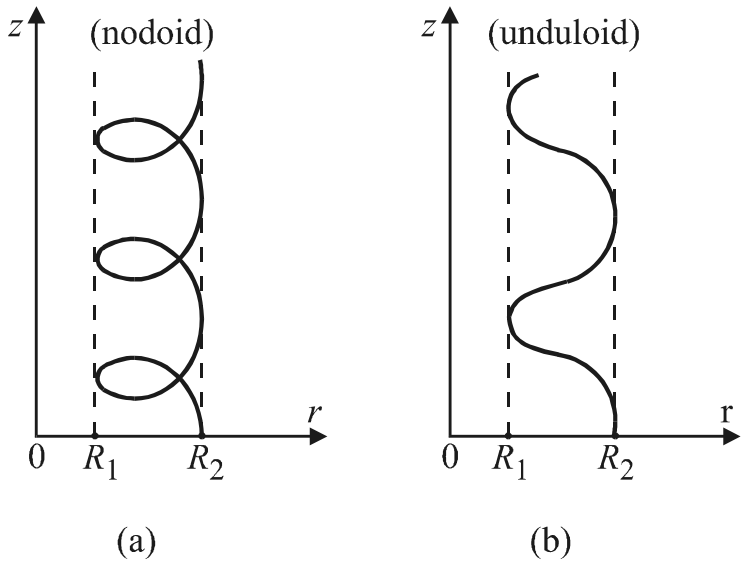

Fig. 2.7. Typical shape of the curves of Plateau: (a) nodoid, (b) unduloid. The curves are confined between two cylinders of radii R_1 and R_2.

In the special case $k_1 r_0 = 1$ the meniscus is spherical. In the other special case, $k_1 r_0 = 0$, the meniscus has the shape of *catenoid*, i.e.

$$z = \pm r_0 \ln\left[r/r_0 + \sqrt{(r/r_0)^2 - 1} \right], \qquad (k_1 = 0) \tag{2.49}$$

Qualitatively, the catenoid looks like the meniscus depicted in Fig. 2.6a; it corresponds to zero capillary pressure and zero mean curvature of the interface ($P_c = 0$ and $H = 0$). In this case $H = 0$ because the two principle curvatures have equal magnitude, but opposite sign, at each point of the catenoid. This is the reason why it is called also “pseudosphere”.

The meniscus has a "neck" (Fig. 2.6a) when $k_1 r_0 \in (-\infty, 1/2)$; in particular, the generatrix is nodoid for $k_1 r_0 \in (-\infty, 0)$, catenoid for $k_1 r_0 = 0$, and unduloid for $k_1 r_0 \in (0, 1/2)$. For the configuration depicted in Fig. 2.6a one has $r_1 > r_0$ (in Fig. 2.7 $R_1 = r_0$, $R_2 = r_1$) and Eq. (2.48) can be integrated to yield

$$z(r) = \pm\left\{ r_0 \mathrm{F}(\phi_1, q_1) + r_1 \operatorname{sgn} k_1 \left[\mathrm{E}(\phi_1, q_1) - \frac{1}{r r_1} \sqrt{(r^2 - r_0^2)(r_1^2 - r^2)} \right] \right\}, \quad (r_0 \le r \le r_1) \tag{2.50}$$

where sng x denotes the sign of x, $q_1 = (1 - r_0^2/r_1^2)^{1/2}$, $\sin\phi_1 = q_1^{-1}(1 - r_0^2/r^2)^{1/2}$; $\mathrm{F}(\phi, q)$ and $\mathrm{E}(\phi, q)$ are the standard symbols for elliptic integrals, respectively, of the first and the second kind [5,17,18]:

$$\mathrm{F}(\phi, q) = \int_0^{\phi} \frac{d\psi}{\sqrt{1 - q^2 \sin^2\psi}}, \qquad \mathrm{E}(\phi, q) = \int_0^{\phi} \sqrt{1 - q^2 \sin^2\psi}\, d\psi \tag{2.51}$$

A convenient numerical method for computation of $\mathrm{F}(\phi, q)$ and $\mathrm{E}(\phi, q)$ is the method of the arithmetic-geometric mean, see Ref. [18], Chapter 17.6.

The meniscus has a "haunch" (Fig. 2.6b) when $k_1 r_0 \in (1/2, +\infty)$; in particular, the generatrix is unduloid for $k_1 r_0 \in (1/2, 1)$, circumference for $k_1 r_0 = 1$, and nodoid for $k_1 r_0 \in (1, +\infty)$. For the configuration depicted in Fig. 2.6b one has $r_0 > r_1$ (in Fig. 2.7 $R_1 = r_1$, $R_2 = r_0$) and Eq. (2.48) can be integrated to yield

$$z(r) = \pm\left[(r_0 - 1/k_1)\mathrm{F}(\phi_2, q_2) - r_0\, \mathrm{E}(\phi_2, q_2) \right], \qquad (r_1 \le r \le r_0) \tag{2.52}$$

where $q_2 = (1 - r_1^2/r_0^2)^{1/2}$, $\sin\phi_2 = q_2^{-1}(1 - r^2/r_0^2)^{1/2}$. More about capillary bridges can be found in Chapter 11. Equation (2.52) has been also used [26,27] to describe the shape of drops and blood cells entrapped in liquid films.

2.3. FORCE BALANCE AT A THREE-PHASE-CONTACT LINE

2.3.1. EQUATION OF YOUNG

As discussed in Section 2.1.2, the Laplace equation is a differential equation, which needs boundary conditions to obtain an uniquely defined solution for the shape of the interface. In Section 2.1.1 we demonstrated that the Laplace equation can be derived as a necessary condition for minimum of the grand thermodynamic potential Ω by using variations in the meniscus shape $u(x,y)$ at *fixed* boundaries. In addition, the boundary conditions for Laplace equation can be derived in a similar way by using variations in the meniscus shape at *mobile* boundaries, see e.g. [8,32-34].

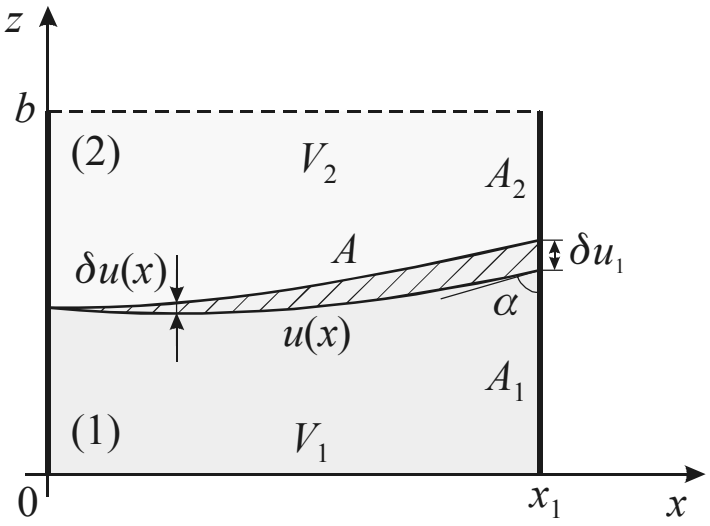

Fig. 2.8. Sketch of a two-phase system composed of phases 1 and 2 occupying volumes V_1 and V_2 separated by an interface of equation $z = u(x)$; A_1 and A_2 are the contact areas of the respective phases with the right-hand side wall; α is contact angle; $\delta u(x)$ and δu_1 represent variation in the shape of the interface and in the position of the contact line, respectively.

Let us consider again a two-phase system closed in a box of volume $V = V_1 + V_2$, see Fig. 2.8. For the sake of simplicity, let us assume that the meniscus has a translational symmetry along the y-axis; then the meniscus profile is $z = u(x)$. Let the right-hand-side wall of the box (Fig. 2.8) be a vertical solid plate situated at $x = x_1$. We consider variations, $\delta u(x)$, of the meniscus profile for movable contact line at the vertical wall at $x = x_1$. The grand potential Ω can be expressed in the form

$$\Omega = -\int_{V_1} P_1 dV - \int_{V_2} P_2 dV + \sigma A + \sigma_{1s} A_1 + \sigma_{2s} A_2 \tag{2.53}$$

where A_1 and A_2 are the contact areas of the vertical wall with phase 1 and 2, respectively (Fig. 2.8); σ_{1s} and σ_{2s} can be interpreted as surface excess densities of Ω for the boundaries solid / phase 1 and solid / phase 2. Since the meniscus has translational symmetry, one can write

$$\int_{V_1} P_1(z) dV = l \int_0^{x_1} dx \int_0^{u(x)} dz P_1(z), \qquad \int_{V_1} P_2(z) dV = l \int_0^{x_1} dx \int_{u(x)}^{b} dz P_2(z), \tag{2.54}$$

where l is the length of the meniscus along the y-axis; $z = 0$ and $z = b$ are the lower and the upper side of the box (Fig. 2.8). The area of the boundary between phases 1 and 2 is

$$A = l\int_0^{x_1} dx\sqrt{1+u_x^2}, \qquad u_x \equiv \frac{\partial u}{\partial x} \tag{2.55}$$

Let the variation $\delta u(x)$ of the meniscus profile is accompanied by a variation δu_1 of the position of the contact line at the vertical wall at $x = x_1$. Then $\delta A_1 = -\delta A_2 = l\,\delta u_1$ and in view of Eqs. (2.53)–(2.55) the first variation of the grand potential Ω can be expressed in the form:

$$\delta\Omega = l\int_0^{x_1}(\delta L)\,dx + (\sigma_{1s} - \sigma_{2s})l\delta u_1 \tag{2.56}$$

where

$$L(u,u_x) \equiv -\int_0^u P_1(z)\,dz - \int_u^b P_2(z)\,dz + \sigma\sqrt{1+u_x^2} \tag{2.57}$$

Differentiating Eq. (2.57) one obtains

$$\delta L = \frac{\partial L}{\partial u}\delta u + \frac{\partial L}{\partial u_x}\frac{d(\delta u)}{dx} \tag{2.58}$$

Next, we integrate by parts the last term in Eq. (2.58):

$$\int_0^{x_1}\frac{\partial L}{\partial u_x}\frac{d(\delta u)}{dx}dx = \left(\frac{\partial L}{\partial u_x}\right)_{x=x_1}\delta u_1 - \int_0^{x_1}\frac{d}{dx}\left[\left(\frac{\partial L}{\partial u_x}\right)\right]\delta u\,dx \tag{2.59}$$

Combining Eqs. (2.56)–(2.59) one derives

$$\delta\Omega = l\int_0^{x_1}\left[\frac{\partial L}{\partial u} - \frac{d}{dx}\left(\frac{\partial L}{\partial u_x}\right)\right]\delta u\,dx + \left[\left(\frac{\partial L}{\partial u_x}\right)_{x=x_1} + \sigma_{1s} - \sigma_{2s}\right]l\,\delta u_1 \tag{2.60}$$

We already know that the meniscus profile satisfies the Laplace equation, Eq. (2.21), which is equivalent to the equation $\dfrac{\partial L}{\partial u} - \dfrac{d}{dx}\left(\dfrac{\partial L}{\partial u_x}\right) = 0$. Hence, the integral term in Eq. (2.60) is equal to zero. Furthermore, the necessary condition for minimum is $\delta\Omega = 0$, and δu_1 is an independent and arbitrary variation. Then the term multiplying δu_1 in Eq. (2.60) must be equal to zero:

$$\left(\frac{\partial L}{\partial u_x}\right)_{x=x_1} + \sigma_{1s} - \sigma_{2s} = 0 \tag{2.61}$$

Using Eq. (2.57) and the identity $u_x = \tan\varphi$, where φ is the running slope angle, one can derive:

$$\frac{\partial L}{\partial u_x} = \frac{\sigma u_x}{\sqrt{1+u_x^2}} = \frac{\sigma \tan\varphi}{\sqrt{1+\tan^2\varphi}} = \sigma \sin\varphi \tag{2.62}$$

Finally, in Eq. (2.62) we set $x = x_1$ and take into account that $(\sin\varphi)_{x=x_1} = \cos\alpha$, where α is the contact angle (Fig. 2.8); then Eq. (2.61) transforms into the Young [35] equation:

$$\sigma_{2s} = \sigma_{1s} + \sigma\cos\alpha \qquad \text{(Young equation)} \tag{2.63}$$

An equivalent equation has been obtained by Dupré [36] in his analysis of the work of adhesion. We derived Eq. (2.63) for the special case of meniscus of translational symmetry, however, this equation has the same form for arbitrarily shaped meniscus and solid surface, see e.g. Ref. [8].

The above derivation of Young equation, which is similar to the derivation of Laplace equation in Section 2.1.1, implies that the Young equation expresses the balance of forces per unit *length* of a three-phase-contact line, likewise the Laplace equation expresses the force balance per unit *area* of a phase boundary. According to Gibbs [29] σ_{1s} and σ_{2s} can be interpreted as surface tensions (forces per unit area): σ_{1s} and σ_{2s} oppose every increase of the "wet" area (without any deformation of the solid) in the same way as σ opposes every dilatation of the interface between fluids 1 and 2; Gibbs termed σ_{1s} and σ_{2s} "superficial tensions".

Equation (2.63), presented in the form $\cos\alpha = (\sigma_{2s} - \sigma_{1s})/\sigma$, shows that the contact angle α can be expressed in terms of the three surface tensions, which in their own turn are determined by the excess molecular interactions in the zone of the phase boundaries (Section 1.1.1). Therefore, the magnitude of the equilibrium contact angle is determined by the intermolecular forces.

It is worth noting that $\delta\Omega = 0$ is only a necessary, but not sufficient, condition for a minimum of the grand potential Ω. This condition is fulfilled also in the case of maximum and inflection

point of Ω. Quite surprisingly, Eriksson & Ljunggren [37] established that for gas bubbles attached to a hydrophobic wall the Young equation can correspond to a maximum of Ω, i.e. to a state of unstable equilibrium. Further, in Ref. [38] the conditions for stable or unstable attachment of a fluid particle (drop, bubble) to a solid wall have been examined.

The force interpretation of the Young equation is illustrated in Fig. 2.9a. One sees that Eq. (2.63) represents the horizontal projection of the vectorial force balance

$$\underline{\boldsymbol{\sigma}} + \underline{\boldsymbol{\sigma}}_{1s} + \underline{\boldsymbol{\sigma}}_{2s} + \mathbf{f}_{\mathrm{R}} = \mathbf{0} \tag{2.64}$$

where the underlined sigma's denote vectors, each of them being tangential to the respective interface and normal to the contact line; $\mathbf{f}_{\mathrm{R}}$ is the vector of the bearing reaction, which is normal to the surface of the solid substrate and counterbalances the vertical projection of the meniscus surface tension:

$$f_{\mathrm{R}} = \sigma \sin\alpha \tag{2.65}$$

Equation (2.65) can be useful in the analysis of the forces applied to a particle, which is attached to an interface (see below). Note that the thermodynamic interpretations of σ, σ_{1s} and σ_{2s} as surface excess densities of the grand thermodynamic potential Ω are completely compatible with their mechanical interpretation as forces per unit length (Fig. 2.9a) insofar as boundaries of a liquid phase are considered and deformations of the solid walls are neglected. These two interpretations (as energy per unit area and force per unit length) are mutually complementary, in spite of the fact that some authors favor the thermodynamic and other ones – the mechanical interpretation. As already mentioned, Gibbs [29] interpreted σ_{1s} and σ_{2s} as tensions opposing the increase of the wet area on the solid surface without any deformation of the solid. On the other hand, differences between energy per unit area and force per unit length appear if deformations of the solid surface take place, see e.g. Refs. [39-43]. Then the force per unit length becomes a two-dimensional *tensor*, whereas the energy per unit area remains a *scalar*, and consequently, these two quantities cannot be equal; the trace of the tensor (the surface tension of the solid) is related to the excess surface energy per unit area by means of the Shuttleworth equation [39-43]. Deformations of the solid phase are out of the conventional capillary hydrostatics and thermodynamics, and will not be considered here.

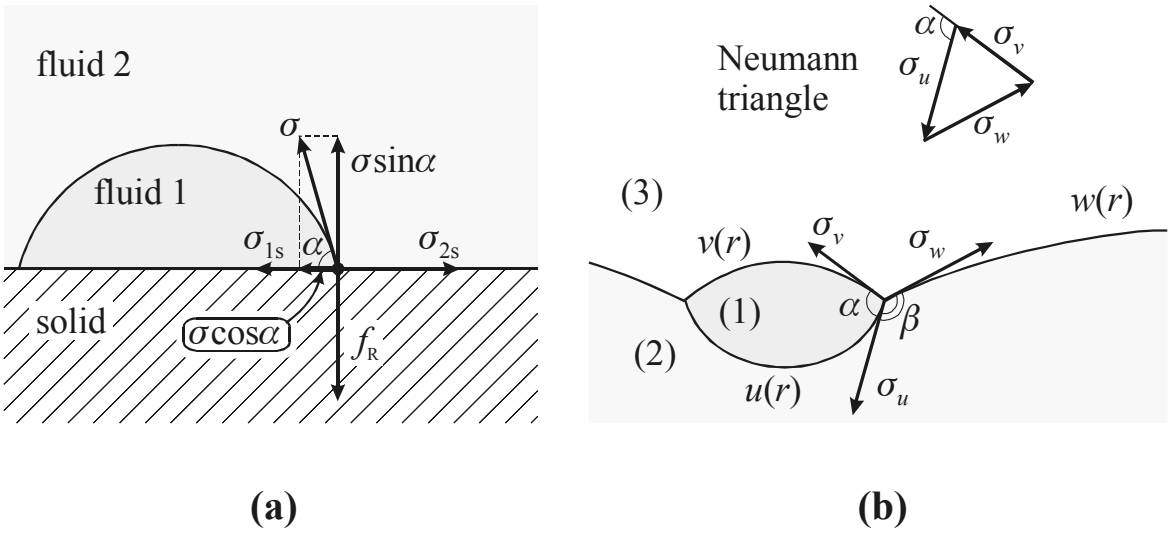

Fig. 2.9. Force interpretation of (a) Young equation (2.64) and (b) the Neumann triangle (2.66); f_R is the bearing reaction of the solid substrate, which counterbalances the normal projection of the surface tension, $\sigma\sin\alpha$; α and β are contact angles.

2.3.2. TRIANGLE OF NEUMANN

Three-phase-contact line can be formed also when all the three phases are *fluid*: such is the line of intersection of the menisci $u(r)$, $v(r)$ and $w(r)$ in Fig. 2.3 (drop or bubble attached to an interface) and Fig. 2.9b (liquid lens at a fluid phase boundary). In this case one can prove (again by a variational method, see e.g. Refs. [32,33]) that the force balance per unit length of the contact line is given by the Neumann [44] vectorial triangle:

$$\underline{\boldsymbol{\sigma}}_u + \underline{\boldsymbol{\sigma}}_v + \underline{\boldsymbol{\sigma}}_w = \mathbf{0}, \qquad \text{(Neumann triangle)} \qquad (2.66)$$

see Fig. 2.9b and Refs. [3,31,45,46]. In this case there are two independent contact angles: α and β. Applying the known cosine theorem to the triangle in Fig. 2.9b one obtains:

$$\sigma_w^2 = \sigma_u^2 + \sigma_v^2 + 2\sigma_u\sigma_v\cos\alpha\,, \qquad \sigma_v^2 = \sigma_u^2 + \sigma_w^2 + 2\sigma_u\sigma_w\cos\beta\,, \qquad (2.67)$$

From Eq. (2.67) one determines [3,46-48]

$$\cos\alpha = \frac{\sigma_w^2 - \sigma_u^2 - \sigma_v^2}{2\sigma_u\sigma_v}, \qquad \cos\beta = \frac{\sigma_v^2 - \sigma_u^2 - \sigma_w^2}{2\sigma_u\sigma_w} \qquad (2.68)$$

Equations (2.68) relate the contact angles α and β to the three interfacial tensions. Hence, we again arrive to the conclusion that the magnitude of the contact angles is determined by the intermolecular forces (which determine also the values of the sigma's) and, moreover, the contact angles do not depend on applied external fields such as gravitational or centrifugal. Note however, that if a line tension is present at the contact line (Section 2.3.3), the contact angle becomes (in principle) dependent on applied external fields as proven by Ivanov et al. [32].

It must be emphasized that the above conclusions related to the physical nature of the contact angles are valid only for the true, i.e. correctly defined, contact angles. Experimentally, by means of some optical method the shapes of the interfaces at some distance from the contact line are usually determined, and then by *extrapolating* them until they intersect the contact angle is found, for review see e.g. Refs. [30,49,50]. The first problem encountered when this procedure is carried out in practice is that the minimum distance from the contact line, at which one can still obtain *experimental* information about the interfacial shape, is limited by the magnification of the microscope [51]. The second problem is related to the transition region in a narrow vicinity of the contact line in which the interactions between the three neighboring phases affect the interfacial tensions and the shape of the interfaces. Although the width of the transition region (it was estimated to 1 μm in Ref. [52]) is smaller than the resolution of the optical methods, if some of the experimental points happen to lie there, this will again affect the extrapolation procedure, and hence – the value of the *macroscopic* contact angle.

The only way to avoid these two errors is [32]: (i) to make sure that all experimental points used lie outside of the transition region and (ii) to carry out the extrapolation of the surface in such a way that its shape at all points satisfies the Laplace equation with the macroscopic value of the surface tension.

2.3.3. THE EFFECT OF LINE TENSION

As discussed above, the true thermodynamic contact angle is subtended between the *extrapolated* surfaces, which obey the Laplace equation. On the other hand, the interactions between the phases (the disjoining pressure effects) in a vicinity of the three-phase-contact line may lead to a deviation of the real interfacial shape from the extrapolated surface and to a variation of the interfacial tensions in this narrow region. In such a case, to make the idealized system (composed of uniform bulk phases and interfaces obeying the Laplace equation at constant surface tension) equivalent to the real system, some excesses of the thermodynamic parameters can be ascribed to the three-phase contact line. The excess linear density of the grand thermodynamic potential Ω has the meaning of a *line tension*, likewise the excess surface density of Ω is identified as the surface tension, see e.g. Ref. [53]. Furthermore, the line tension can be interpreted as a force, directed tangentially to the contact line, just like the tension of a stretched fiber or string [54].

For the first time the concept of line tension was formulated by Gibbs [29] in his theory of capillarity. The thermodynamic theory of systems with line tension was developed by Buff and Saltsburg [45], and Boruvka and Neumann [53]. The theory of line tension for systems containing thin liquid film was worked out in Refs. [52,55,56]. Following Veselovsky and Pertsov [54], let us consider a small circular portion (arc) of a curved contact line with length s, curvature radius r_c and line tension κ, which is depicted in Fig. 2.10. The considered portion of the contact line is situated symmetrically with respect to the x-axis, which is chosen to pass through the center of curvature O. Due to the action of line tension, a force of magnitude κ and direction tangential to the contact line is exerted at both ends of the considered arc (Fig. 2.10). Then one obtains

$$s = 2\theta r_c\,, \qquad |f_x| = 2\kappa \sin\theta \tag{2.69}$$

where f_x is the sum of the x-projections of the two forces due to the line tension. Then it turns out that the existence of line tension leads to the appearance of a force

$$\sigma_\kappa \equiv \lim_{\theta\to 0} \frac{|f_x|}{s} = \frac{\kappa}{r_c} \tag{2.70}$$

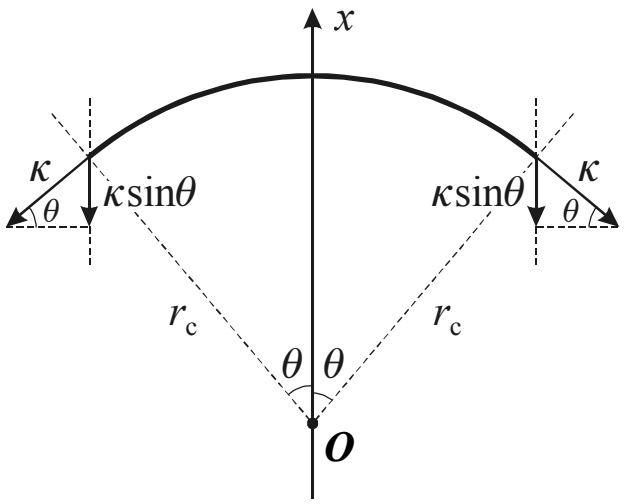

Fig. 2.10. The line tension κ, acting tangentially to a small portion (arc) of a curved contact line, leads to the appearance of a force per unit length $\sigma_\kappa = \kappa/r_c$, which is directed toward the center of curvature of the arc, point O; r_c is the curvature radius of the considered elementary arc of the contact line.

acting per unit length of the contact line. In each point of the contact line this force, $\underline{\boldsymbol{\sigma}}_\kappa$, is directed toward the center of curvature (toward the center of the circumference, if the contact line is circular). The above derivation is valid for any smooth curved line, insofar as every small portion of such a line can be approximated with an arc of circumference [7].

If the effect of line tension is included into the Young equation, Eqs. (2.63) and (2.64) acquire the more general form [57]:

$$\sigma_{2s} = \sigma_{1s} + \sigma\cos\alpha + \frac{\kappa}{r_c} \tag{2.71}$$

$$\underline{\boldsymbol{\sigma}} + \underline{\boldsymbol{\sigma}}_{1s} + \underline{\boldsymbol{\sigma}}_{2s} + \underline{\boldsymbol{\sigma}}_\kappa + \mathbf{f}_R = \mathbf{0} \tag{2.72}$$

In this case the contact line belongs to a solid surface and the force interpretation of κ and $\underline{\boldsymbol{\sigma}}_\kappa$ is similar to the interpretation of $\underline{\boldsymbol{\sigma}}_{1s}$ and $\underline{\boldsymbol{\sigma}}_{2s}$ given by Gibbs (see above); in particular, κ can be interpreted as a force, which opposes the extension of the perimeter of the wet zone in every process of variation of the wet area *without any deformation* in the solid substrate.

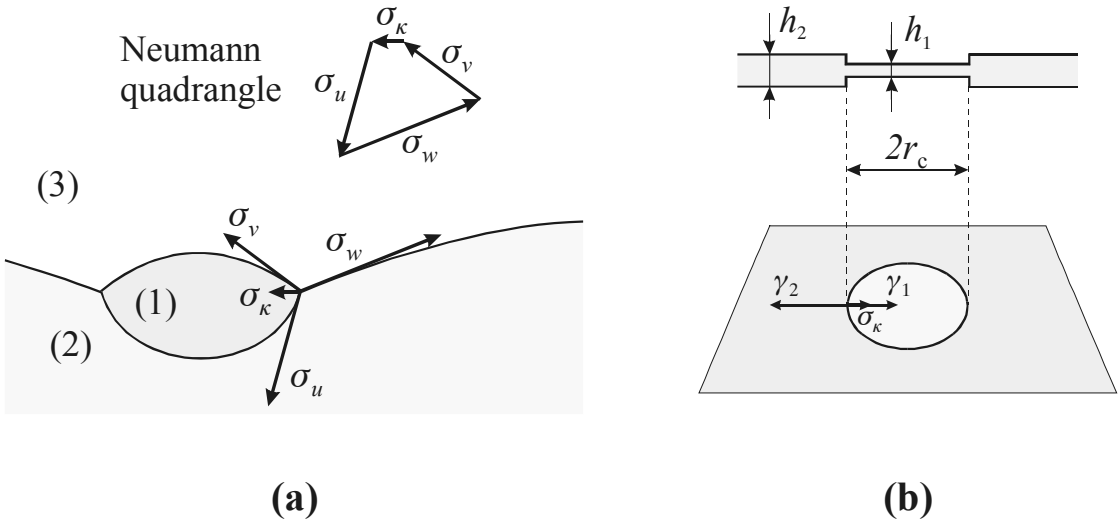

Fig. 2.11. Balance of forces per unit length of the contact line (a) around a floating lens (b) around a spot of tension γ_1 and thickness h_1 in a liquid film of tension γ_2 and thickness h_2; σ_κ is the contribution of line tension.

Likewise, the Neumann triangle, Eq. (2.66) transforms into a "Neumann quadrangle" defined by the following vectorial equation [32,48,58-60]

$$\underline{\boldsymbol{\sigma}}_u + \underline{\boldsymbol{\sigma}}_v + \underline{\boldsymbol{\sigma}}_w + \underline{\boldsymbol{\sigma}}_\kappa = \mathbf{0}, \tag{2.73}$$

see Fig. 2.11a. Note that Eq. (2.73) can be derived from the thermodynamic condition for minimum of the thermodynamic potential [32,33]. To do that the capillary system is considered as being built up from *bulk* (three-dimensional) phases, *surface* (two-dimensional) phases and *line* (one-dimensional) phases [53,60]. Then the grand potential is expressed in the form:

$$\Omega = -\sum_i P_i V_i + \sum_m \sigma_m A_m + \sum_n \kappa_n L_n \tag{2.74}$$

where the indices "i", "m" and "n" numerate the bulk, surface and line phases; as usual, P denotes pressure, V – volume, σ – surface tension, A – area, κ – line tension and L – length.

Next, let us consider a circular spot of radius r_c, thickness h_1 and tension γ_1 formed in a foam (or emulsion) film of thickness h_2 and tension γ_2, see Fig. 2.11b. Such spots are typical for the transition from primary to secondary film (from common black to Newton black film) in foams

[25,61,62], as well as for the multiple step-wise transitions in the thickness of liquid films containing surfactant micelles or other spherical colloid particles [63,64]. The force balance per unit length of the line encircling the spot is (Fig. 2.11b):

$$\frac{\kappa}{r_c} = \gamma_2 - \gamma_1 \tag{2.75}$$

Equation (2.75) is obviously a linear counterpart of the Laplace equation (2.4). One could estimate the magnitude of κ for the spot in Fig. 2.11b in the following way [64]. The periphery of the spot can be approximated with a step of total height $\Delta h = h_2 - h_1$. The excess energy due to the formation of the spot is $\kappa \approx \sigma \Delta h$, where σ is the surface tension of the film. Thus with typical values $\sigma = 36$ mN/m and $\Delta h = 5$ nm one calculates $\kappa \approx 1.8 \times 10^{-10}$ N. It should be noted that this estimate is pertinent to the system depicted in Fig. 2.11b, and it is certainly irrelevant for other systems and/or configurations. What concerns the sign of κ, it must be positive if the shape of the spot is circular. Indeed, at $\kappa > 0$ each deviation from circular shape (at constant spot area) would lead to an increase of the length, L, of the contact line encircling the spot and of the line energy, κL; therefore, the spot will spontaneously acquire a circular shape, which minimizes the line energy. Such circular spots are observed also in adsorption monolayers of insoluble molecules, like phospholipids, which exhibit coexisting domains of different two-dimensional phases [65-67]. In some cases, however, the boundaries between such coexisting domains are highly irregular and unstable, which can be attributed (at least in part) to the action of negative line tension. Note, that in (physically) two-dimensional systems, like the film in Fig, 2.11b, there is no other force, but a *positive* line tension, which tends to keep the shape of the contact line circular. That is the reason why the line tension is an effect of primary importance for such "two-dimensional" systems, in which the contact line separates *two* surface phases (Fig. 2.11b).

Quite different is the case of a *three*-phase-contact line, see Fig. 2.11a and Eq. (2.73). In order to minimize the surface area (and energy) the fluid interfaces acquire axisymmetric shape and their lines of intersection (the three-phase-contact lines) are usually circumferences. Then even a negative line tension cannot disturb the regular shape of the contact line, which is preserved by the surface tensions in the Young equation (2.71) and Neumann quadrangle (2.73). The

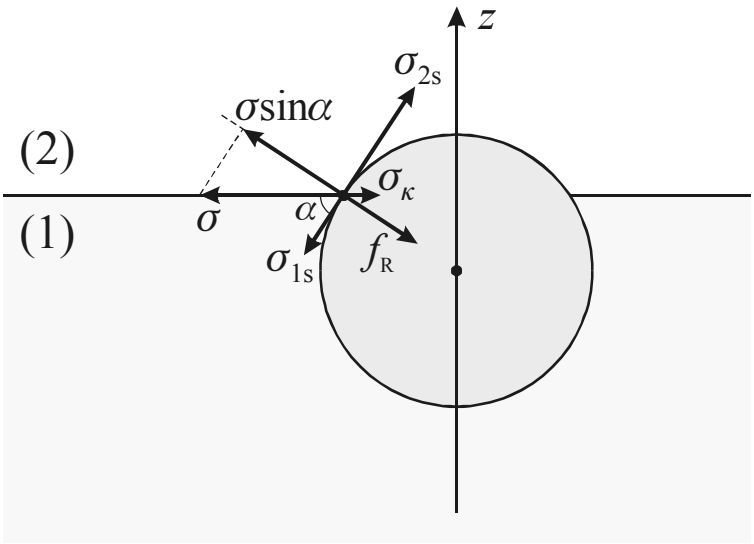

Fig. 2.12. Balance of forces per unit length of the contact line of a small solid sphere attached to the planar interface between the fluid phases 1 and 2; σ is the interfacial tension, σ_{1s} and σ_{2s} are the two solid-fluid tensions, σ_κ is the line tension effect, f_R is the bearing reaction of the solid particle: $f_R + \sigma_\kappa \sin\alpha = \sigma \sin\alpha$.

accumulated results for three-phase systems show that the line-tension term turns out to be only a small correction, which can be (and is usually) neglected in Eqs. (2.71)–(2.73), see Section 2.3.4.

As an example for application of the Young equation (2.72) let us consider a small spherical particle attached to the interface between two fluid phases, Fig. 2.12. We presume that the weight of the particle is small and the particle does not create any deformation of the fluid interface [68,69]. All forces taking part in Eq. (2.72) are depicted in Fig. 2.12, including the normal projection, $\sigma\sin\alpha$, of the interfacial tension. Its tangential projection, $\sigma\cos\alpha$, is counterbalanced by $\sigma_{2s} + \sigma_\kappa \cos\alpha - \sigma_{1s}$ in accordance with the Young equation. Then one could conclude (erroneously!) that $\sigma\sin\alpha$ and/or $\sigma_\kappa \sin\alpha$, which have non-zero projections along the z-axis (Fig. 2.12), give rise to a force acting on the particle along the normal to the fluid interface. If such a force were really operative, it would create a deformation of the fluid interface around the particle, which would be in contradiction with the experimental observations. Then a question arises: how to calculate correctly the net force exerted on a fluid particle attached to an interface at equilibrium?

The rule (called sometimes the principle of Stevin), stems from the classical mechanics and it is the following: The net force exerted on a particle originates only from phases, which are *outer* with respect to the given particle: the pressure of an outer bulk phase, the surface tension of an outer surface phase and the line tension of an outer line phase. (For example, if a particle is hanging on a fiber, then the tension of the fiber has to be considered as the line tension of an "outer line phase".)

In our case (the particle in Fig. 2.12) the *outer* forces are the pressures in the two neighboring fluid phases 1 and 2, and the surface tension, σ, of the boundary between them. The integral effect of their action gives a zero net force for the configuration depicted in Fig. 2.12 due to its symmetry. Then there is no force acting along the normal to the interface and the latter will not undergo a deformation in a vicinity of the particle. (Such a deformation would appear if the particle weight and the buoyancy force were not negligible.)

On the other hand, the solid-fluid tensions, σ_{1s} and σ_{2s}, the tension σ_κ due to line tension, and the bearing reaction of the solid, f_R, cannot be considered as outer forces. However, σ_{1s}, σ_{2s} and σ_κ also affect the equilibrium position of the particle at the interface insofar as they (together with σ) determine the value of the contact angle α, see Eq. (2.71).Additional information can be found in Chapter 5 below, where balances of forces experienced by particles attached to the boundary between two fluids are considered.

2.3.4. HYSTERESIS OF CONTACT ANGLE AND LINE TENSION

The experimental determination of line tension is often based on the fact, that the presence of a κ/r_c term in Eqs. (2.71) and (2.73) leads (in principle) to a dependence of the contact angle α on the radius of the contact line r_c (σ, σ_{1s} and σ_{2s} are presumably constants), see Refs. [70-79]. However, there is another phenomenon, the hysteresis of contact angle, which also leads to variation of the contact angle, see e.g. Ref. [80]. Both phenomena may have a similar physical origin [75].

The fact that a hysteresis of contact angle takes place with liquid menisci on a *solid* substrate has been known for a long time [81,82]. It is an experimental fact that a range of stable contact angles can be measured on a real solid surface. The highest of them is termed "advancing", and

the lowest one – "receding" contact angle. The difference between the advancing and receding angles is called "the range of hysteresis", or shortly, "hysteresis" [83,84]. The widely accepted qualitative explanation of this phenomenon is that the hysteresis is caused by the presence of surface roughness and chemical heterogeneity of the real solid surfaces [75, 85-96]. From this viewpoint, the Young equation is believed to be valid only for an ideal solid surface, which is molecularly smooth, chemically homogeneous, rigid and insoluble [84].

However, hysteresis of contact angle can be observed even on an ideal solid surface if a thin liquid film is formed in front of an advancing meniscus, or left behind a receding meniscus; this was proven theoretically by Martynov et al. [97], see also Refs. [98,99]. In this case the hysteresis is due to the action of an adhesive surface force within the thin film, which opposes the detachment of the film surfaces and facilitates their attachment. Such forces are present (and hysteresis is observed) not only in wetting films on a solid substrate, but also in free foam and emulsion films stabilized by usual surfactants [100-102] or by proteins [99]. It turns out that, as a rule, one observes hysteresis of contact angle and only with some special systems hysteresis is completely missing. Such special systems can be liquid lenses on a fluid interface [30, 103-107] or thin films without strong adhesive forces [108].

The occurrence of hysteresis is different for a completely *fluid* three-phase-contact line and for a three-phase contact involving one *solid* phase: In the former case at complete equilibrium (immobile contact line) an equilibrium contact angle is established [99-102]; in contrast, in the latter case (in the presence of solid phase) it is practically impossible to figure out which angle, could be identified as the equilibrium one within the range between the receding and advancing angles.

Coming back to the line tension issue, in Fig. 2.13 we demonstrate, that in some cases the line tension could be a manifestation of the hysteresis of contact angle. Let us assume that for some value of the contact angle, $\alpha = \alpha_1$, the Young equation (2.63) is satisfied (Fig. 2.13a). Due to the hysteresis another metastable contact angle, α_2, exists ($\alpha_2 > \alpha_1$, see Fig. 2.13b). From a macroscopic viewpoint the force balance in Fig. 2.13b can be preserved if only a line tension term, $\sigma_\kappa = \kappa/r_c$, is introduced, see Eq. (2.71) with $\alpha = \alpha_2$. Indeed, the surface tensions σ, σ_{1s}

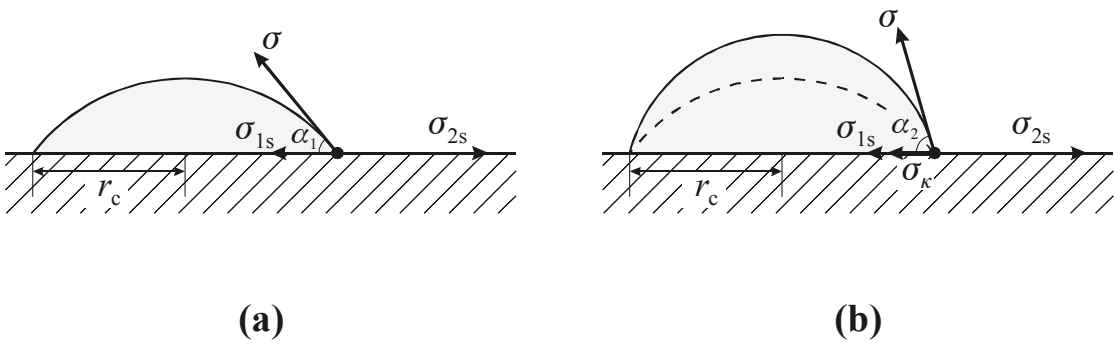

Fig. 2.13. Sessile liquid drop on a solid substrate. (a) Balance of the forces acting per unit length of the contact line, of radius r_c; σ is the surface tension of the liquid, σ_{1s} and σ_{2s} are the tensions of the two solid-fluid interfaces, α_1 is contact angle. (b) After liquid is added to the drop, hysteresis is observed: the contact angle rises to α_2 at fixed r_c; the fact that the macroscopic force balance is preserved (the contact line remains immobile) can be attributed to the action of a line tension effect σ_κ.

and σ_{2s} are the same in Figs. 2.13a and 2.13b, and the difference between the contact angles ($\alpha_2 > \alpha_1$) can be attributed to the action of a line tension.

The interpretation of the contact-angle hysteresis as a line tension could be accepted, because, as already mentioned, the two phenomena have a similar physical origin: local microscopic deviations from the *macroscopic* Young-Laplace model in a narrow vicinity of the contact line. When the meniscus advance is accompanied by an *increase* of the contact radius r_c, a *positive* line tension must be included in the Young equation to preserve the force balance (Fig. 2.13b). In the opposite case, if the meniscus advance is accompanied by a *decrease* of r_c, then a *negative* line tension must be included in the Neumann-Young equation to preserve the force balance. The shrinking bubbles, like that depicted in Fig. 2.3, correspond to the latter case and, really, negative line tensions have been measured with such bubbles [109,110, 100-102]; see also the discussion in Ref. [111].

Theoretical calculations, which do not take into account effects such as surface roughness or heterogeneity, or dynamic effects with adhesive thin films, usually predict very small values of the line tension from 10^{-11} to 10^{-13} N, see Table 2.1. On the contrary, the experiments which deal with real solid surfaces, or which are carried out under dynamic conditions, as a rule give much higher values of κ (Table 2.1). The values of κ in a given experiment often have variable magnitude, and even – variable sign [70-73,100-102,109,110]. Moreover, the values of κ

determined in different experimental and theoretical works vary with 8 orders of magnitude (Table 2.1).

Table 2.1. Comparison of experimental and theoretical results for line tension κ.

Researchers	Theory / Experiment	System	Value(s) of line tension κ (N)
Tarazona & Navascues [112]	Theory	Solid-liquid-vapor contact line	-2.6 to -8.2×10^{-11}
Navascues & Mederos [113]	Experiment	Nucleation rate of water drops on Hg	-2.9 to -3.9×10^{-10}
de Feijter & Vrij [52]	Theory	Foam films	$\approx -1 \times 10^{-12}$
Kolarov & Zorin [114]	Experiment	Foam films	-1.7×10^{-10}
Denkov et al. [115]	Theory	Emulsion films	-0.95 to -1.57×10^{-13}
Torza and Mason [59]	Experiment	Emulsion films	-0.6 to -5.8×10^{-8}
Ivanov & coworkers [100-102, 109-111]	Experiment	Foam film at the top of shrinking bubbles	-1×10^{-7} to ≈ 0
Wallace & Schürch [116,117]	Experiment	Sessile drop on monolayer	$+1$ to $+2.4 \times 10^{-8}$
Neumann & coworkers [118-121]	Experiment	Sessile drops	$+1$ to $+6 \times 10^{-6}$
Gu, Li & Cheng [122]	Experiment	Interface around a cone	$\approx +1 \times 10^{-6}$
Nguyen et al. [123]	Experiment	Silanated glass spheres on water-air surface	$+1.2$ to $+5.5 \times 10^{-6}$

There could be some objections against the formal treatment of the contact angle hysteresis as a line-tension effect. Firstly, some authors [124-126] interpret the hysteresis as an effect of static friction (overcoming of a barrier), which is physically different from the conventional molecular interpretation of line tension, see e.g. Ref. [112]. Secondly, a hysteresis of contact angle can be observed also with a *straight* contact line ($r_c \to \infty$); if such hysteresis is interpreted as a line tension effect, one will obtain $\kappa \to \infty$, but $\sigma_\kappa = \kappa / r_c$ will remain finite.

If σ_κ in the Neumann "quadrangle", Eq. (2.73), is a manifestation of hysteresis, then σ_κ is not expected to vary significantly with the size of the particles (solid spheres, drops, bubbles, lenses). On the other hand, r_c can vary with many orders of magnitude. Consequently, if the line tension effect in some system is a manifestation of a contact angle hysteresis, then one could expect that the measured $|\kappa| = |\sigma_\kappa| r_c$ will be larger for the larger particles (greater r_c) and smaller for the smaller particles (smaller r_c). Some of the reported experimental data (Table 2.1) actually exhibit such a tendency. For example, in the experiments of Neumann and coworkers [118-121] and Gu et al. [122] $r_c \approx 3$ mm and one estimates an average value $\sigma_\kappa \approx$ 1 mN/m; in the experiments of Ivanov and coworkers [100-102,109,110] the mean value of the contact radius is $r_c \approx 35$ μm and one estimates $|\sigma_\kappa| \approx 1.4$ mN/m; in the experiment of Torza & Mason [59] $r_c \approx 15$ μm in average and then $|\sigma_\kappa| \approx 2$ mN/m; in the experiments of Navascues & Mederos [113] $r_c \approx 23$ nm and one obtains $|\sigma_\kappa| \approx 20$ mN/m. One sees, that in contrast with $|\kappa|$, which varies with many orders depending on the experimental system, $|\sigma_\kappa|$ exhibits a relatively moderate variation. Then a question arises whether κ or σ_κ is a better material parameter characterizing the linear excess at the three-phase contact line.

In the experiments with slowly diminishing bubbles from solutions of ionic surfactant [100-102] it has been firmly established that the shrinking of the contact line is accompanied by a rise (hysteresis) of the contact angle, α, and appearance of a significant negative line tension, κ. When the shrinking of the contact line was stopped (by control of pressure), both α and $|\kappa|$ relaxed down to their equilibrium values, which for κ turned out to be zero in the framework of the experimental accuracy ($\pm 1.5 \times 10^{-8}$ N). This effect was interpreted [100-102,111] as a "dynamic" line tension related to local deformations in the zone of the contact line, which are due to the action of attractive (adhesive) forces opposing the detachment of the film surfaces in the course of meniscus advance. Arguments in favor of such an interpretation are that a measurable line tension effect is missing in the case of (i) receding meniscus (expanding bubbles) [100-102] and (ii) shrinking bubbles from *nonionic* surfactant solution [108]. In the latter case the adhesive surface forces in the film are negligible.

Finally, let us summarize the conclusions stemming from the analysis of the available experimental and theoretical results for the line tension:

1) The line tension of *three*-phase-contact-lines can vary by many orders of magnitude depending on the specific system, configuration (contact-line radius) and process (static or dynamic conditions). The sign of line tension could also vary, even for similar systems [70-73]. In some cases this could be due to the fact, that the measured line tension is a manifestation of hysteresis of contact angle; in this case the variability of the magnitude and sign of the line tension is connected with the indefinite value of the contact angle. Hence, unlike the surface tension, the line tension, κ, strongly depends on the geometry of the system and the occurrence of dynamic processes. This makes the theoretical prediction of line tension a very hard task and limits the importance and the applicability of the experimentally determined values of κ only to the given special system, configuration and process.

2) The line tension of *three*-phase-contact lines is usually a small correction (an effect of secondary importance) in the Young equation or Neumann triangle, and it could be neglected without a great loss of accuracy.

3) In contrast, the line tension of the boundary between *two* surface phases (see e.g. Fig. 2.11b) is an effect of primary importance, which determines the shape and the stability of the boundaries between domains (spots) in thin liquid films and Langmuir adsorption films.

2.4. SUMMARY

The pressure exhibits a jump on the two sides of a curved interface or membrane of non-zero tension. This effect is quantitatively described by the Laplace equation, which expresses the force balance per unit area of a curved interface. In general, the Laplace equation is a second order nonlinear partial differential equation, Eq. (2.20), determining the shape of the interface. This equation, however, reduces to a much simpler ordinary differential equation for the practically important special case of axisymmetric interfaces and membranes, see Eqs. (2.22)–(2.25). There are three types of axisymmetric menisci. (I) Meniscus meeting the axis of revolution: the shapes of sessile and pendant drops and some configurations of biological cells belong to this type (Section 2.2.1). (II) Meniscus decaying at infinity: it describes the shape of the fluid interface around a vertical cylinder, floating solid or fluid particle (including gas bubble and oil lens), as well as around a hole in a wetting film (Section 2.2.2). (III) Meniscus

confined between two cylinders (Section 2.2.3): in the absence of gravitational deformation the shape of such a meniscus is described by the classical curves "nodoid" and "unduloid", which represent linear combinations of the two elliptic integrals of Legendre; such menisci are the capillary "bridges", the Plateau borders in foams, the shape of the free surface of a fluid particle or biological cell pressed between two plates. For all types of axisymmetric menisci the available analytical formulas are given, and numerical procedures are recommended if there is no appropriate analytical expression.

In reality the fluid interfaces (except those of free drops and bubbles) are bounded by three-phase contact lines. The values of the contact angles subtended between three intersecting phase boundaries are determined by the force balance at the contact line, which is termed Young equation in the case of solid particle, Eq. (2.64), and Neumann triangle in the case of fluid particle, Eq. (2.66). It is demonstrated that the force balance at the contact line (likewise the Laplace equation) can be derived by variation of the thermodynamic potential. Linear excess energy (line tension) can be ascribed to a contact line. The line tension can be interpreted as a force tangential to the contact line, which is completely similar to the tension of a stretched string of fiber from mechanical viewpoint. When the contact line is curved, the line tension gives a contribution, σ_κ, in the Young and Neumann equations, see Figs. 2.10, 2.11a and Eqs. (2.72) and (2.73). The latter equations express force balances, which influence the equilibrium position of a particle at an interface. The rule how to calculate the net force exerted on such a particle is presented and illustrated, see Fig. 2.12.

The accumulated experimental results for various systems show that the line tension a of three-phase-contact line can vary by many orders of magnitude, and even by sign, depending on the specific system, configuration and process. In some cases the measured macroscopic line tension can be a manifestation of contact angle hysteresis; in such a case the variability of the magnitude and sign of the line tension is connected with the indefinite value of the contact angle. The line tension of *three*-phase-contact-lines (see Table 2.1) is usually dominated by the surface tensions of the adjacent interfaces, and therefore it is a small correction in the Young equation or Neumann triangle. In contrast, the line tension of the boundary between *two* surface phases (see Fig. 2.11b and Eq. 2.75) is an effect of primary importance, which determines the shape and the stability of the respective contact lines.

2.5. REFERENCES

1. P.S. Laplace, Traité de mécanique céleste; suppléments au Livre X, 1805.
2. S. Ono, S. Kondo, Molecular theory of surface tension in liquids, in: S. Flügge (Ed.), Handbuch der Physik, vol. 10, Springer, Berlin, 1960, p. 134.
3. J.S. Rowlinson, B. Widom, Molecular Theory of Capillarity, Clarendon Press, Oxford, 1982.
4. J. Gaydos, The Laplace Equation of Capillarity, in: D. Möbius, R. Miller (Eds.) "Drops and Bubbles in Interfacial Research", Elsevier, Amsterdam, 1998.
5. G.A. Korn, T.M. Korn, Mathematical Handbook, McGraw-Hill, New York, 1968.
6. G. Arfken, Mathematical Methods for Physicists, Academic Press, London, 1970.
7. A.J. McConnell, Application of Tensor Analysis, Dover, New York, 1957.
8. R. Finn, Equilibrium Capillary Surfaces, Springer-Verlag, New York, 1986.
9. L.D. Landau, E.M. Lifshitz, Fluid Mechanics, Pergamon Press, Oxford, 1984.
10. H.M. Princen, The Equilibrium Shape of Interfaces, Drops, and Bubbles, in: E. Matijevic, (Ed.) Surface and Colloid Science, Vol. 2, Wiley, New York, 1969, p. 1.
11. S. Hartland, R.W. Hartley, Axisymmetric Fluid-Liquid Interfaces, Elsevier, Amsterdam, 1976.
12. P.A. Kralchevsky, K.D. Danov, N.D. Denkov, Chemical Physics of Colloid Systems and Interfaces, in: K.S. Birdi (Ed.) Handbook of Surface and Colloid Chemistry, CRC Press, Boca Raton, 1997.
13. A.W. Adamson, Physical Chemistry of Surfaces, Wiley, New York, 1976.
14. P.A. Kralchevsky, I.B. Ivanov, A.D. Nikolov, J. Colloid Interface Sci. 112 (1986) 108.
15. P.A. Kralchevsky, A.S. Dimitrov, K. Nagayama, J. Colloid Interface Sci. 160 (1993) 236.
16. P. Concus, J. Fluid Mech. 34 (1968) 481.
17. E. Jahnke, F. Emde, F. Lösch, Tables of Higher Functions, McGraw-Hill, New York, 1960.
18. M. Abramowitz, I.A. Stegun, Handbook of Mathematical Functions, Dover, New York, 1965.
19. B.V. Derjaguin, Dokl. Akad. Nauk SSSR 51 (1946) 517.
20. L.L. Lo, J. Fluid. Mech. 132 (1983) 65.
21. S.B.G. O'Brien, J. Colloid Interface Sci. 183 (1996) 51.
22. A. Scheludko, D. Exerowa, Kolloid-Z. 165 (1959) 148.

23. A. Scheludko, Proc. Koninkl. Nederl. Akad. Wet., B65 (1962) 87.

24. A. Scheludko, Adv. Colloid Interface Sci. 1 (1967) 391.

25. K.J. Mysels, J. Phys. Chem. 68 (1964) 3441.

26. A. Hadjiiski, R. Dimova, N.D. Denkov, I.B. Ivanov, R. Borwankar, Langmuir 12 (1996) 6665.

27. I.B. Ivanov, A. Hadjiiski, N.D. Denkov, T.D. Gurkov, P.A. Kralchevsky, S. Koyasu, Biophys. J. 75 (1998) 545.

28. J. Plateau, Mem. Acad. Roy. Soc. Belgique 33 (1861), sixth series and preceding papers.

29. J.W. Gibbs, The Scientific Papers of J.W. Gibbs, Vol. 1, Dover, New York, 1961.

30. A.S. Dimitrov, P.A. Kralchevsky, A.D. Nikolov, D.T. Wasan, Colloids Surf. 47 (1990) 299.

31. G. Bakker, Kapillarität und Oberflächenspannung, in: Handbuch der Experimentalphysik, Band 6, Akademische Verlagsgesellschaft, Leipzig, 1928.

32. I.B. Ivanov, P.A. Kralchevsky, A.D. Nikolov, J. Colloid Interface Sci. 112 (1986) 97.

33. J. Gaydos, A.W. Neumann, Thermodynamics of Axisymmetric Capillary Systems, in: A.W. Neumann & J.K. Spelt (Eds.) Applied Surface Thermodynamics, Marcel Dekker, New York, 1996, p. 53.

34. S. Ljunggren, J.C. Eriksson, P.A. Kralchevsky, J. Colloid Interface Sci. 191 (1997) 424.

35. T. Young, Philos. Trans. Roy. Soc. London 95 (1805) 55.

36. A. Dupré, Theorie Mecanique de la Chaleur, Paris, 1869, p. 368.

37. J.C. Eriksson, S. Ljunggren, Langmuir 11 (1995) 2325.

38. P.A. Kralchevsky, Langmuir 12 (1996) 5951.

39. R. Shuttleworth, Proc. Phys. Soc. (London) A63 (1950) 444.

40. C. Herring, in: W.E. Kingston (Ed.) The Physics of Powder Metallurgy, McGraw-Hill, New York, 1951.

41. G.C. Benson, K.S. Yun, in: E.A. Flood (Ed.) The Solid-Gas Interface, Vol. 1, Marcel Dekker, New York, 1967.

42. J.C. Eriksson, Surface Sci. 14 (1969) 221.

43. A.I. Rusanov, Kolloidn. Zh. 39 (1977) 711; J. Colloid Interface Sci. 63 (1978) 330.

44. F.E. Neumann, in: A. Wangerin (Ed.) Vorlesungen über die Theorie der Kapillarität, Teubner, Leipzig, 1894, p. 161.

45. F.P. Buff, H. Saltsburg, J. Chem. Phys. 26 (1957) 23.

46. F.P. Buff, in: S. Flügge (Ed.) Encyclopedia of Physics, Vol. 10, Springer, Berlin, 1960, 298.

47. N.F. Miller, J. Phys. Chem. 45 (1941) 1025.

48. P.R. Pujado, L.E. Scriven, J. Colloid Interface Sci. 40 (1972) 82.

49. P.A. Kralchevsky, K.D. Danov, I.B. Ivanov, Thin Liquid Film Physics, in: R.K. Prud'homme (Ed.) Foams: Theory, Measurements and Applications, Marcel Dekker, New York, 1995, Section 3.3.

50. J.K. Spelt, E.I. Vargha-Butler, Contact Angle and Liquid Surface Tension Measurements, in: A.W. Neumann & J.K. Spelt (Eds.) Applied Surface Thermodynamics, Marcel Dekker, New York, 1996, p. 379.

51. B.A. Pethica, J. Colloid Interface Sci. 62 (1977) 567.

52. J.A. de Feijter, A. Vrij, J. Electroanal. Chem. Interfacial Electrochem. 37 (1972) 9.

53. L. Boruvka, A.W. Neumann, J. Chem. Phys. 66 (1977) 5464.

54. V. S. Veselovsky, V. N. Pertsov, Z. Phys. Khim. 8 (1936) 245.

55. I.B. Ivanov, B.V. Toshev, B.P. Radoev, in: J.F. Padday (Ed.) Wetting, Spreading and Adhesion, Academic Press, New York, 1978, p. 37.

56. G.A. Martynov, I.B. Ivanov, B.V. Toshev, Kolloidn. Zh. 38 (1976) 474.

57. B.A. Pethica, Rep. Prog. Appl. Chem. 46 (1961) 14.

58. A.I. Rusanov, Phase Equilibria and Surface Phenomena, Khimia, Leningrad, 1967 (in Russian); Phasengleichgewichte und Grenzflächenerscheinungen, Akademie Verlag, Berlin, 1978.

59. S. Torza, S.G. Mason, Kolloid-Z. Z. Polym. 246 (1971) 593.

60. I.B. Ivanov, P.A. Kralchevsky, in: I.B. Ivanov (Ed.) Thin Liquid Films, Marcel Dekker, New York, 1988, p. 91.

61. P.M. Kruglyakov, in: I.B. Ivanov (Ed.) Thin Liquid Films, Marcel Dekker, New York, 1988, p. 767.

62. D. Exerowa, P.M. Kruglyakov, Foam and Foam Films, Elsevier, Amsterdam, 1998.

63. A.D. Nikolov, D.T. Wasan, P.A. Kralchevsky, I.B. Ivanov, Ordered Structures in Thinning Micellar Foam and Latex Films, in: N. Ise and I. Sogami (Eds.) Ordering and Organisation in Ionic Solutions , World Scientific, Singapore, 1988, p. 302.

64. P.A. Kralchevsky, A.D. Nikolov, D.T. Wasan, I.B. Ivanov, Langmuir 6 (1990) 1180.

65. H. Möhwald, Annu. Rev. Phys. Chem. 41 (1990) 441.

66. U. Retter, K. Siegler, D. Vollhardt, Langmuir 12 (1996) 3976.

67. M.J. Roberts, E.J. Teer, R.S. Duran, J. Phys. Chem. B 101 (1997) 699.

68. V.N. Paunov, P.A. Kralchevsky, N.D. Denkov, K. Nagayama, J. Colloid Interface Sci. 157 (1993) 100.

69. R. Aveyard, B.P. Binks, P.D.I. Fletcher, C.E. Rutherford, Colloids Surf. A 83 (1994) 89.

70. A.B. Ponter, A.P. Boyes, Canadian J. Chem. 50 (1972) 2419.

71. A.P. Boyes, A.B. Ponter, J. Chem. Eng. Japan 7 (1974) 314.

72. A.B. Ponter, M. Yekta-Fard, Colloid Polym. Sci. 263 (1985) 1.

73. M. Yekta-Fard, A.B. Ponter, J. Colloid Interface Sci. 126 (1988) 134.

74. D. Platikanov, M. Nedyalkov, V. Nasteva, J. Colloid Interface Sci. 75 (1980) 620.

75. J. Gaydos, A.W. Neumann, Line Tension in Multiphase Equilibrium Systems, in: A.W. Neumann & J.K. Spelt (Eds.) Applied Surface Thermodynamics, Marcel Dekker, New York, 1996, p. 169.

76. D. Li, Colloids Surf. A 116 (1996) 1.

77. J. Drelich, Colloids Surf. A 116 (1996) 43.

78. Y. Gu, D. Li, P. Cheng, Colloids Surf. A 122 (1997) 135.

79. A. Marmur, Colloids Surf. A 136 (1998) 81.

80. R.J. Good, M.N. Koo, J. Colloid Interface Sci. 71 (1979) 283.

81. N.K. Adam, The Physics and Chemistry of Surfaces, Oxford University Press, Oxford, 1941.

82. R. Shuttleworth, G.L.J. Bailey, Discuss. Faraday Soc. 3 (1948) 16.

83. R.E. Johnson Jr., R.H. Dettre, in: E. Matijevic (Ed.) Surface and Colloid Science, Vol. 2, Wiley, New York, 1969, p. 85.

84. A. Marmur, Adv. Colloid Interface Sci. 50 (1994) 121.

85. F.Z. Preisach, Z. Phys. 94 (1935) 277.

86. D.H. Everett, W.I. Whitton, Trans. Faraday Soc. 48 (1952) 749.

87. R.J. Good, J. Phys. Chem. 74 (1952) 5041.

88. J.A. Enderby, Trans. Faraday Soc. 51 (1955) 835.

89. R.E. Johnson Jr., R.H. Dettre, J. Phys. Chem. 68 (1964) 1744.

90. T.D. Blake, J.M. Haynes, in: J.F. Danielli et al. (Eds.) Progress in Surface and Membrane Science, Vol. 6, Academic Press, 1973, p. 125.

91. J.D. Eick, R.J. Good, A.W. Neumann, J. Colloid Interface Sci. 53 (1975) 235.

92. A.W. Neumann, in: J.F. Padday (Ed.) Wetting, Spreading and Adhesion, Academic Press, New York, 1978, p. 3.

93. R.J. Good, in: R.J. Good & R.R. Stromberg (Eds.) Surface and Colloid Science, Vol. 11, Plenum Press, 1979, p. 1.

94. I.D. Mayergoyz, Mathematical Models of Hysteresis, Springer-Verlag, New York, 1991.

95. A. Marmur, J. Colloid Interface Sci. 168 (1994) 40.

96. J. Drelich, J.D. Miller, R.J. Good, J. Colloid Interface Sci. 179 (1996) 37.

97. G.A. Martynov, V.M. Starov, N.V. Churaev, Kolloidn. Zh. 39 (1977) 472.

98. V.M. Starov, Adv. Colloid Interface Sci. 39 (1992) 147.

99. K.D. Danov, P.A. Kralchevsky, I.B. Ivanov, Chapter 9 in: G. Broze (Ed.) Handbook of Detergents, Part A.: Properties, Surfactant Science Series, Vol. 82. Marcel Dekker, New York, 1999, Section V.C.

100. I.B. Ivanov, A.S. Dimitrov, A.D. Nikolov, N.D. Denkov, P.A. Kralchevsky, J. Colloid Interface Sci. 151 (1992) 446.

101. A.S. Dimitrov, A.D. Nikolov, P.A. Kralchevsky, I.B. Ivanov, J. Colloid Interface Sci. 151 (1992) 462.

102. I.B. Ivanov, P.A. Kralchevsky, A.S. Dimitrov, A.D. Nikolov, Adv. Colloid Interface Sci. 39 (1992) 77.

103. J. Mingins, A.D. Nikolov, Ann. Univ. Sofia Fac. Chem. 75 (1981) 3.

104. R. Aveyard, J.H. Clint, J. Chem. Soc. Faraday Trans. 93 (1997) 1397.

105. A. Dussaud, M. Vignes-Adler, Langmuir 13 (1997) 581.

106. P. Chen, S.S. Susnar, A. Amirfazli, C. Mak, A.W. Neumann, Langmuir 13 (1997) 3035.

107. P. Chen, S.S. Susnar, C. Mak, A. Amirfazli, A.W. Neumann, Colloids Surf. A 129 (1997) 45.

108. L.A. Lobo, A.D. Nikolov, A.S. Dimitrov, P.A. Kralchevsky D.T. Wasan, Langmuir 6 (1990) 995, Figs. 10 and 13.

109. P.A. Kralchevsky, A.D. Nikolov, I.B. Ivanov. J. Colloid Interface Sci. 112 (1986) 132.

110. A.D. Nikolov, P.A. Kralchevsky, I.B. Ivanov. A New Method for Measuring Film and Line Tensions, in: K.L. Mittal & P. Bothorel (Eds.) Surfactants in Solution, Vol. 6, Plenum Press, New York, 1987, p. 1537.

111. T.D. Gurkov, P.A. Kralchevsky, J. Disp. Sci. Technol. 18 (1997) 609.

112. P. Tarazona, G. Navascues, Physica A 115 (1982) 490.

113. G. Navascues, L. Mederos, Surf. Technol. 17 (1982) 79.

114. T. Kolarov, Z.M. Zorin, Colloid J. USSR 42 (1980) 899.

115. N.D. Denkov, D.N. Petsev, K.D. Danov, J. Colloid Interface Sci., 176 (1995) 189.

116. J.A. Wallace, S. Schürch, J. Colloid Interface Sci. 124 (1988) 452.

117. J.A. Wallace, S. Schürch, Colloids Surf. 43 (1990) 207.

118. J. Gaydos, A.W. Neumann, J. Colloid Interface Sci. 120 (1987) 76.

119. D. Li, A.W. Neumann, Colloids Surf. 43 (1990) 195.

120. D. Duncan, D. Li, J. Gaydos, A.W. Neumann, J. Colloid Interface Sci. 169 (1995) 256.

121. A. Amirfazli, D.Y. Kwok, J. Gaydos, A.W. Neumann, J. Colloid Interface Sci. 205 (1998) 1.

122. Y. Gu, D. Li, P. Cheng, J. Colloid Interface Sci. 180 (1996) 212.

123. A.V. Nguyen, H. Stechemesser, G. Zobel, H.J. Schulze, J. Colloid Interface Sci. 187 (1997) 547.

124. R. Finn, M. Shinbrot, J. Math. Anal. Appl. 123 (1987) 1.

125. S.D. Iliev, J. Colloid Interface Sci. 194 (1997) 287.

126. S.D. Iliev, J. Colloid Interface Sci. 213 (1999) 1.